The Astrophysical Journal, 614:472–489, 2004 October 10

TIME-DISTANCE HELIOSEISMOLOGY: NOISE ESTIMATION

L. Gizon and A. C. Birch
W. W. Hansen Experimental Physics Laboratory, Stanford University, Stanford, CA 94305
Received 2004 March 31; accepted 2004 June 5

ABSTRACT

As in global helioseismology, the dominant source of noise in time-distance helioseismology measurements is realization noise due to the stochastic nature of the excitation mechanism of solar oscillations. Characterizing noise is important for the interpretation and inversion of time-distance measurements. In this paper we introduce a robust definition of travel time that can be applied to very noisy data. We then derive a simple model for the full covariance matrix of the travel-time measurements. This model depends only on the expectation value of the filtered power spectrum and assumes that solar oscillations are stationary and homogeneous on the solar surface. The validity of the model is confirmed through comparison with *SOHO* MDI measurements in a quiet-Sun region. We show that the correlation length of the noise in the travel times is about half the dominant wavelength of the filtered power spectrum. We also show that the signal-to-noise ratio in quiet-Sun travel-time maps increases roughly as the square root of the observation time and is at maximum for a distance near half the length scale of supergranulation.

Subject headings: methods: data analysis — Sun: granulation — Sun: helioseismology — Sun: interior — Sun: oscillations — waves

1. INTRODUCTION

The purpose of time-distance helioseismology (Duvall et al. 1993) is to infer the local structure and dynamics of the solar interior by measuring and interpreting the travel times of solar waves between different locations on the Sun's surface. Although the foundations of time-distance helioseismology have not been written in a consistent form yet, the essential steps that need to be followed are well known. First, we must have a well-defined and meaningful procedure to measure travel times (and other quantities) from the observed cross-covariances. Second, we must derive the equations that connect the observations to perturbations in internal solar properties with respect to a solar model: the linear forward problem. Third, we must solve these integral equations to infer solar internal properties: the inverse problem.

In global helioseismology, it is well understood that the precision of the measurement of the pulsation frequencies is affected by realization noise resulting from the stochastic nature of the excitation of solar oscillations (e.g., Woodard 1984; Duvall & Harvey 1986; Schou 1992; Libbrecht 1992; Toutain & Appourchaux 1994). Little is known, however, of the properties of the noise in time-distance helioseismology measurements. It is important to study these properties, since the presence of noise affects all three steps mentioned above: the travel-time measurement procedure must be robust with respect to noise, the forward problem must be solved for the agreed on definition of travel time, and the correlations in the measurements must be taken into account in the inversion procedure. Ultimately, a good understanding of the noise properties is required to assign correct errors on the solar perturbations inferred through time-distance helioseismology.

In a commonly used averaging scheme, temporal cross-covariances are constructed between the Doppler signal observed at a given location on the Sun and a concentric annulus (Duvall et al. 1993, 1996). Center-to-annulus wave travel times are traditionally measured by fitting a Gaussian wavelet to the cross-covariances (e.g., Kosovichev & Duvall 1997). Baudin & Korzennik (1998) attempted to estimate the noise level in travel times through Monte Carlo simulations; unfortunately, they assumed that the noise in the cross-covariances could be modeled by additive uncorrelated Gaussian noise (temporal bins are in fact highly correlated). They pointed out that fits to the cross-covariances may not converge for short observation times. An interesting approach, pioneered by Jensen et al. (2003), consists of estimating the noise directly from the data by measuring the rms travel time within a quiet-Sun region. The underlying assumptions are that the fluctuations in the travel times are dominated by noise, not by "real" solar signals, and that the travel times measured at different locations can be seen as different realizations of the same random process. By real solar signals we mean travel-time perturbations due to inhomogeneities in the solar interior that are slowly varying over the time of the observations. Jensen et al. (2003) studied the correlation between the travel times as a function of the distance between the central points, at fixed annular radius. Their method, however, remains to be proved to be correct and has no predictive power.

The main purpose of this paper is to derive a model for the noise covariance matrix of the travel times; this model can be evaluated for different spatial separations and for various averaging schemes (annuli, quadrants, point-to-point) and travel-time types (mean, difference, one-way). The organization of the paper is as follows: We begin with a new robust definition of travel times that can be applied to very noisy cross-covariances, i.e., when the observing time T is short and when spatial averaging is minimal. For the sake of simplicity, we do not fit for the amplitude of the cross-covariance and restrict our attention to quiet-Sun data. Using *SOHO* MDI data we estimate the covariance of travel times using the method of Jensen et al. (2003). We then derive a model for the covariance of travel times due to realization noise. We assume that the wave field is stationary and homogeneous over a small region in Cartesian geometry. In this model, travel-time fluctuations are only due to the stochastic nature of the wave field, and the noise falls off as $T^{-1/2}$. We find excellent agreement

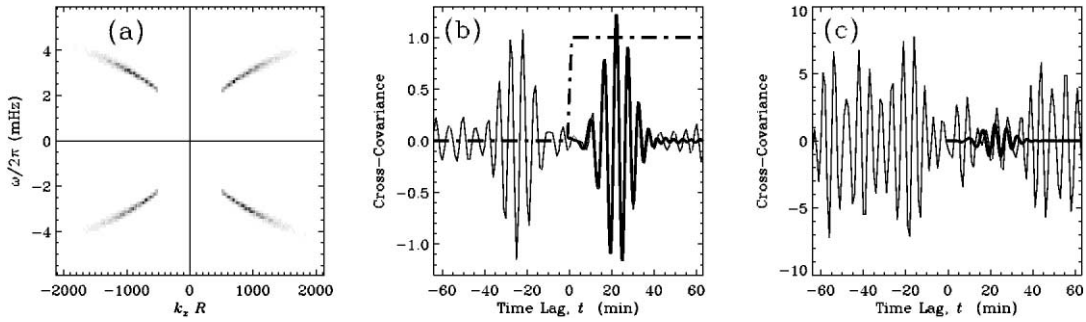

FIG. 1.—The *f*-mode power and cross-covariance functions. (*a*) Cut through the filtered power spectrum at $k_y = 0$. The filter only allows power near the *f*-mode ridge. (*b*) Spatially averaged cross-covariance function (*thin line*) for $\boldsymbol{\Delta} = \boldsymbol{x}_2 - \boldsymbol{x}_1 = (10\ \mathrm{Mm})\hat{\boldsymbol{x}}$, where $\hat{\boldsymbol{x}}$ points west. The thick dot-dashed line shows the window function $f(t)$ used in the travel-time measurement procedure (see text). The thick line shows the reference cross-covariance function, $C^{\mathrm{ref.}}$ (*c*) Cross-covariance $C(\boldsymbol{x}_1, \boldsymbol{x}_2, t)$ for a single pair of points (*thin line*). The observation time is $T = 128$ minutes, and the pixel size is $h_x = 0.83$ Mm. Overplotted is the reference cross-covariance C^{ref} from (*b*) (*thick line*). Note the scale difference between (*b*) and (*c*).

between the data and the model for short observation times and without spatial averaging, i.e., when the fluctuations in the data are dominated by realization noise. For larger T or with annular averaging, there are extra correlations in the data introduced by real solar perturbations (e.g., supergranulation) that do not follow the $T^{-1/2}$ law. We determine the signal-to-noise ratio in travel-time measurements for the quiet Sun. We believe that our simple formula for the noise covariance matrix can be used reliably in future inversions of quiet-Sun point-to-point travel times. For the case of point-to-annulus travel time measurements we find that Monte Carlo simulations of the noise covariance are more accurate than simple analytical approximations.

2. ROBUST TRAVEL TIME MEASUREMENTS

Let us denote by $\phi(\boldsymbol{x}, t)$ the filtered oscillation signal observed at point $\boldsymbol{x}$ and time t, where the filter acts by multiplication in the Fourier domain. In this paper we consider two types of filters: an *f*-mode filter that removes all power away from the *f*-mode ridge (Fig. 1*a*) and a Gaussian phase-speed filter for *p*-modes (Fig. 2*a*). The signal is sampled at times $t_i = ih_t$ over a time interval of length T, where $h_t = 1$ minute is the sampling rate and i is an integer in the range $-N/2 \leq i < N/2$. In this paper we define the temporal cross-covariance function between points $\boldsymbol{x}_1$ and $\boldsymbol{x}_2$ as

$$C(\boldsymbol{x}_1,\ \boldsymbol{x}_2,\ t_j) = \frac{h_t}{T - |t_j|} \sum_i \phi(\boldsymbol{x}_1,\ t_i)\phi(\boldsymbol{x}_2,\ t_i + t_j). \quad (1)$$

This definition is slightly modified from the definition of Gizon & Birch (2002) to include the normalization factor $1/(T - |t_j|)$, which becomes significant when T is small. Traditionally, the cross-covariance function has been computed over time intervals $T \sim 8$ hr and averaged spatially over points $\boldsymbol{x}_2$ that belong to an annulus or quadrants centered at $\boldsymbol{x}_1$ (Duvall et al. 1993, 1997). The time interval T puts a limit on the temporal scale of the solar phenomena that can be studied with time-distance helioseismology: the signature of solar features with a lifetime less than T will be reduced because of the temporal averaging. In addition, the spatial averaging may also reduce the ability of time-distance helioseismology to resolve features with small spatial scales. In order to maximize the potential resolution of time-distance helioseismology, we would like to be able to measure travel times from cross-covariances measured with shorter T and with as little spatial averaging as possible. The difficulty with measuring travel times for small T with minimal spatial averaging is that the cross-covariance function can be very noisy. Figure 1*c* shows an example cross-covariance function (for *f*-modes) measured over a time interval $T = 128$ minutes between two pixels (spatial sampling $h_x = 0.83$ Mm). Conventional fitting methods will fail on cross-covariances with this level of noise. Even when the fit converges, for less noisy data, the distribution of the phase travel times will not be a unimodal Gaussian distribution but a periodic distribution with an $\sim$5 minute period (the typical wave period) because the envelope of the cross-covariance is not sufficiently localized in time.

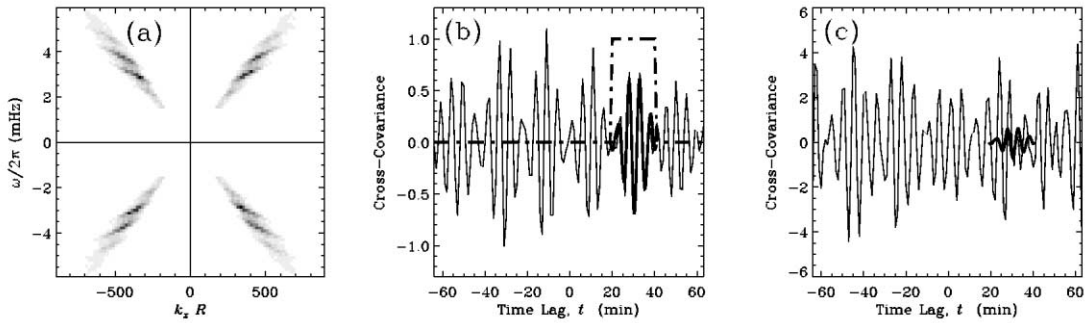

FIG. 2.—The *p*-mode power and cross-covariance functions. (*a*) Cut through the filtered power spectrum at $k_y = 0$. The Fourier filter is a phase speed filter of the form $\exp[-(\omega/k - v)^2/(2s^2)]$, where $v = 36.5$ km s^{-1} and $s = 2.5$ km s^{-1}. The three visible ridges are p_1, p_2, and p_3. (*b*) Spatially averaged cross-covariance function (*thin line*) for $\boldsymbol{\Delta} = \boldsymbol{x}_2 - \boldsymbol{x}_1 = (25\ \mathrm{Mm})\hat{\boldsymbol{x}}$. The thick dot-dashed line shows the window function $f(t)$ used in the travel-time measurement procedure (see text). The thick line shows the reference cross-covariance function, $C^{\mathrm{ref.}}$ (*c*) Cross-covariance $C(\boldsymbol{x}_1, \boldsymbol{x}_2, t)$ for a single pair of points (*thin line*). The observation time is $T = 128$ minutes, and the pixel size is 0.83 Mm. Overplotted is the reference cross-covariance C^{ref} from (*b*) (*thick line*). Note the scale difference between (*b*) and (*c*).

In order to fit cross-covariances that are noisy, we introduce a new definition of travel time. Following a suggestion by T. L. Duvall, Jr. (2002, private communication), we start by constructing a smooth cross-covariance, denoted by C^ϵ, obtained by adding a small fraction ϵ of the observed cross-covariance C to a smooth reference cross-covariance. For ϵ small enough, the function

$$C^\epsilon(\boldsymbol{x}_1,\ \boldsymbol{x}_2,\ t) = \epsilon C(\boldsymbol{x}_1,\ \boldsymbol{x}_2,\ t) + (1-\epsilon)C^{\rm ref}(\boldsymbol{x}_2-\boldsymbol{x}_1,\ t) \quad (2)$$

is well behaved and can be fitted with standard techniques. Here ϵ is a free parameter that is less than 1 and greater than 0. The reference cross-covariance $C^{\rm ref}$ can, for example, be computed from a standard solar model. For cross-covariances that have little noise, the choice $\epsilon = 1$ is reasonable (the standard definition), but as noise increases the parameter ϵ should be reduced.

Let us denote by $\tau_+(\boldsymbol{x}_1, \boldsymbol{x}_2)$ the travel time for waves that move from $\boldsymbol{x}_1$ to $\boldsymbol{x}_2$ and by $\tau_-(\boldsymbol{x}_1, \boldsymbol{x}_2)$ the travel time for waves that move from $\boldsymbol{x}_2$ to $\boldsymbol{x}_1$. To measure the one-way travel times τ_+ and τ_- from C^ϵ, we use a method similar to the one described by Gizon & Birch (2002). As explained in Appendix B, τ_+ is such that it minimizes the "badness of fit" between $C^\epsilon(t)$ and $C^{\rm ref}(t-\epsilon\tau_+)$ computed within a time window $f(t)$. The isolation window $f(t)$, which is 0 for $t<0$, selects an interval around the (first bounce) arrival time of the wave packet. Similarly, τ_- is measured from $C^\epsilon(t)$ within the time window $f(-t)$. Examples of the function $f(t)$ are shown in Figures 1*b* and 2*b*. By choosing the amplitude of $C^{\rm ref}$ to match an estimate of the amplitude of the expectation value of C, the travel times are essentially independent of ϵ for noiseless data. For our definition to be valid whatever the level of noise, we take the limit $\epsilon \to 0$. In this limit, the minimization can be done analytically, and we obtain (see Appendix B)

$$\tau_\pm(\boldsymbol{x}_1,\ \boldsymbol{x}_2) = h_t \sum_t W_\pm(\boldsymbol{x}_2-\boldsymbol{x}_1,\ t) \times \left[C(\boldsymbol{x}_1,\ \boldsymbol{x}_2,\ t) - C^{\rm ref}(\boldsymbol{x}_2-\boldsymbol{x}_1,\ t)\right]. \quad (3)$$

The sum over t is a short notation to mean the sum over all discrete times in the interval $-T/2 \le t < T/2$ (see Appendix A). The weight functions $W_\pm$ are given by

$$W_\pm(\boldsymbol{\Delta},\ t) = \frac{\mp f(\pm t)\dot{C}^{\rm ref}(\boldsymbol{\Delta},\ t)}{h_t \sum_{t'} f(\pm t')\left[\dot{C}^{\rm ref}(\boldsymbol{\Delta},\ t')\right]^2}\ , \quad (4)$$

where $\dot{C}^{\rm ref}$ is the time derivative of $C^{\rm ref}$. For both *f*- and *p*-modes, the functions $C^{\rm ref}$ that we use are very close to the measured spatial averages of C (see Figs. 1*b* and 2*b*). Equation (3) is our definition of travel time for the remainder of this paper.

This definition has a number of useful properties. First, it is very robust with respect to noise. The fit reduces to a simple sum that can always be evaluated whatever the level of noise. Second, it is linear in the cross-covariance. As a consequence, averaging various travel-time measurements is equivalent to measuring a travel time on the average cross-covariance. This is unlike previous definitions of travel time that involve nonlinear fitting procedures. Third, the probability density functions of τ_+ and τ_- are unimodal Gaussian distributions. This means, in particular, that it makes sense to associate an error with a travel-time measurement. Another way to illustrate this point is to plot the distribution of the travel times obtained for different spatial locations $\boldsymbol{x}_1$ at fixed $\boldsymbol{x}_2-\boldsymbol{x}_1$, in a quiet-Sun region. For short T (128 minutes), it is apparent in Figure 3 that travel times are normally distributed. Fourth, our new definition reduces to the definition of Gizon & Birch (2002) when C is noiseless ($T \to \infty$). This means that sensitivity kernels obtained according to the method developed by Gizon & Birch (2002) remain valid with this definition of travel time.

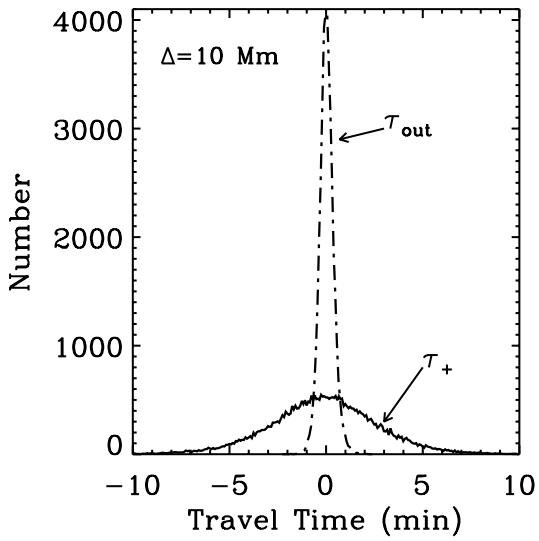

FIG. 3.—Histogram of the observed *f*-mode travel times when the observation time is $T = 128$ minutes. The solid line is for the point-to-point travel times τ_+ measured between pairs of individual pixels separated by $\Delta = 10$ Mm (the pixel size is 0.83 Mm). The distribution of τ_+ is Gaussian with a standard deviation of 2.8 minutes. The dot-dashed line gives the distribution of the point-to-annulus travel times $\tau_{\rm out}$, which is Gaussian with a standard deviation of 22 s.

We note that this simplified definition is only meaningful when the expectation value of the cross-covariance is mostly independent of position at fixed $\boldsymbol{x}_2-\boldsymbol{x}_1$; thus, we restrict the discussion to quiet-Sun data. Our definition could presumably be generalized to fit for the amplitude and other parameters. It would indeed be necessary to fit for the amplitude of the cross-covariance to measure travel times around sunspots.

Throughout the rest of the paper we refer to various combinations of the one-way travel times $\tau_\pm$. The travel-time difference ("diff") and the mean travel time ("mean") are

$$\tau_{\rm diff}(\boldsymbol{x}_1,\ \boldsymbol{x}_2) = \tau_+(\boldsymbol{x}_1,\ \boldsymbol{x}_2) - \tau_-(\boldsymbol{x}_1,\ \boldsymbol{x}_2), \quad (5)$$

$$\tau_{\rm mean}(\boldsymbol{x}_1,\ \boldsymbol{x}_2) = \frac{1}{2}\ [\tau_+(\boldsymbol{x}_1,\ \boldsymbol{x}_2) + \tau_-(\boldsymbol{x}_1,\ \boldsymbol{x}_2)]. \quad (6)$$

In the following we use the short notation $\tau_a(\boldsymbol{x}_1, \boldsymbol{x}_2)$, where the subscript a can be +, −, diff, or mean (for point-to-point measurements).

For the annulus geometry we define the cross-covariance, $C_{\rm ann}(\boldsymbol{x},\ \Delta,\ t)$, obtained by averaging over points that belong to an annulus of mean radius Δ centered at position $\boldsymbol{x}$. More precisely,

$$C_{\rm ann}(\boldsymbol{x},\ \Delta,\ t) = \frac{\sum_{\boldsymbol{r}} \aleph(\|\ \boldsymbol{r}-\boldsymbol{x}\ \| - \Delta) C(\boldsymbol{x},\ \boldsymbol{r},\ t)}{\sum_{\boldsymbol{r}'} \aleph(\|\ \boldsymbol{r}'-\boldsymbol{x}\ \| - \Delta)}, \quad (7)$$

where sums are over all spatial pixels on the solar surface and the spatial weight function $\aleph$ is chosen to be Gaussian:

$$\aleph(x) = e^{-x^2/(2w^2)}. \quad (8)$$

The parameter w fixes the thickness of the annulus, which we choose to be half the pixel size, $w = h_x/2$. Other choices for the function $\aleph$ are possible; for example, Duvall takes $\aleph(x) = 1$ if $|x| < h_x/2$ and 0 otherwise. From the cross-covariance $C_{\rm ann}$, we can define the travel times for waves traveling from the central point to the annulus (out) and from the annulus to the central point (in) as

$$\tau_{\rm out(in)}(\boldsymbol{x};\ \Delta) = h_t \sum_t W_{\rm out(in)}(\Delta,\ t) \times \left[C_{\rm ann}(\boldsymbol{x},\ \Delta,\ t) - C^{\rm ref}_{\rm ann}(\boldsymbol{x},\ \Delta,\ t)\right], \quad (9)$$

where $C^{\rm ref}_{\rm ann}$ is a reference cross-covariance appropriate for the annulus geometry (see Appendix B). For the annulus geometry, the difference ("oi") and mean ("mn") travel times are

$$\tau_{\rm oi}(\boldsymbol{x};\ \Delta) = \tau_{\rm out}(\boldsymbol{x};\ \Delta) - \tau_{\rm in}(\boldsymbol{x};\ \Delta), \quad (10)$$

$$\tau_{\rm mn}(\boldsymbol{x};\ \Delta) = \frac{1}{2}\ [\tau_{\rm out}(\boldsymbol{x};\ \Delta) + \tau_{\rm in}(\boldsymbol{x};\ \Delta)]. \quad (11)$$

In the following we use the short notation $\tau_\alpha(\boldsymbol{x}; \Delta)$, where the subscript α can be out, in, oi, or mn (for annuli).

3. SPATIAL CORRELATIONS OF MDI TRAVEL TIMES

In this section, we consider the method that Jensen et al. (2003) used to estimate noise in the travel times. They estimated travel-time correlations from the data using a spatial average instead of an ensemble average (the idea is that travel times measured for pairs of points that are well separated in space are like independent realizations). This method for estimating noise is only valid when the travel-time fluctuations are completely dominated by realization noise and the perturbations due to real solar signals (e.g., supergranulation) are negligible. As is shown below, this condition is met for small observation times, for instance, $T = 128$ minutes, and point-to-point measurements.

Given any real function Q of horizontal vectors $\boldsymbol{x}, \boldsymbol{x}', \ldots$, we define the spatial average $\langle Q\rangle$ of Q by

$$\langle Q(\boldsymbol{x},\ \boldsymbol{x}',\ \ldots)\rangle = \frac{1}{n} \sum_{\boldsymbol{r}} Q(\boldsymbol{x}+\boldsymbol{r},\ \boldsymbol{x}'+\boldsymbol{r},\ \ldots), \quad (12)$$

where n is the total number of available samples and each sample corresponds to a discrete horizontal offset $\boldsymbol{r}$. For any two real functions X and Y, estimates of the covariance of X and Y, the standard deviation of X, and the correlation coefficient between X and Y are given by

$$\mathrm{Cov}\langle X,\ Y\rangle = \langle XY\rangle - \langle X\rangle\langle Y\rangle, \quad (13)$$

$$\sigma\langle X\rangle = \sqrt{\mathrm{Cov}\langle X,\ X\rangle}, \quad (14)$$

$$\mathrm{Cor}\langle X,\ Y\rangle = \mathrm{Cov}\langle X,\ Y\rangle / (\sigma\langle X\rangle\sigma\langle Y\rangle). \quad (15)$$

In the case of point-to-point travel-time measurements, we consider two pairs of points with coordinates $(\boldsymbol{x}_1,\ \boldsymbol{x}_2)$ and $(\boldsymbol{x}'_1,\ \boldsymbol{x}'_2)$, as depicted in Figure 4*a*. According to the definition of equation (13), the covariance of the travel times estimated by spatial averaging of the data can be written as

$$\mathrm{Cov}^{\rm data}_{a,b}(\boldsymbol{d},\ \boldsymbol{\Delta},\ \boldsymbol{\Delta}') = \mathrm{Cov}\left\langle \tau_a(\boldsymbol{x}_1,\ \boldsymbol{x}_2),\ \tau_b(\boldsymbol{x}'_1,\ \boldsymbol{x}'_2)\right\rangle. \quad (16)$$

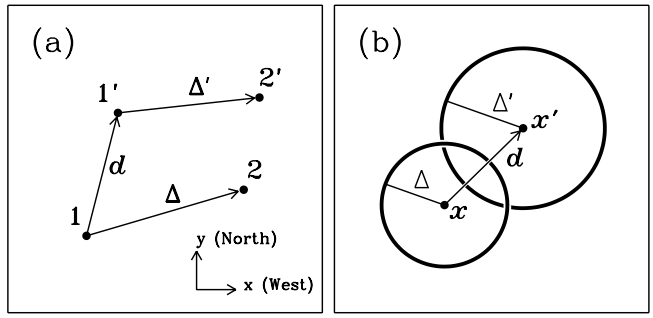

FIG. 4.—(*a*) Geometry for the covariance $\mathrm{Cov}_{a,b}(\boldsymbol{d}, \boldsymbol{\Delta}, \boldsymbol{\Delta}', T)$ for point-to-point measurements. The travel times $\tau_a(\boldsymbol{x}_1, \boldsymbol{x}_2)$ and $\tau_b(\boldsymbol{x}'_1, \boldsymbol{x}'_2)$ are measured between pairs $(\boldsymbol{x}_1, \boldsymbol{x}_2)$ and $(\boldsymbol{x}'_1, \boldsymbol{x}'_2)$. Also shown are the vectors $\boldsymbol{\Delta} = \boldsymbol{x}_2 - \boldsymbol{x}_1$, $\boldsymbol{\Delta}' = \boldsymbol{x}'_2 - \boldsymbol{x}'_1$, and $\boldsymbol{d} = \boldsymbol{x}'_1 - \boldsymbol{x}_1$. (*b*) Geometry for the covariance $\mathrm{Cov}_{\alpha,\beta}(\boldsymbol{d}, \Delta, \Delta', T)$ for center-to-annulus travel times. The travel time $\tau_\alpha(\boldsymbol{x}; \Delta)$ is measured between $\boldsymbol{x}$ and the concentric annulus with radius Δ, and $\tau_\beta(\boldsymbol{x}'; \Delta')$ is measured between $\boldsymbol{x}'$ and the concentric annulus with radius Δ'. Also shown is the vector $\boldsymbol{d} = \boldsymbol{x}' - \boldsymbol{x}$.

The function $\mathrm{Cov}^{\rm data}_{a,b}$ depends on the types of travel times (the indices a and b can be either +, −, mean, or diff), the separation $\boldsymbol{d} = \boldsymbol{x}'_1 - \boldsymbol{x}_1$, the vectors $\boldsymbol{\Delta} = \boldsymbol{x}_2 - \boldsymbol{x}_1$ and $\boldsymbol{\Delta}' = \boldsymbol{x}'_2 - \boldsymbol{x}'_1$, and the duration of the observation T. The computation of $\mathrm{Cov}^{\rm data}_{a,b}$ involves a spatial averaging of the product $\tau_a(\boldsymbol{x}_1, \boldsymbol{x}_2)\tau_b(\boldsymbol{x}'_1,\ \boldsymbol{x}'_2)$ at fixed parameters $\boldsymbol{d}$, $\boldsymbol{\Delta}$, and $\boldsymbol{\Delta}'$. Similarly, we denote the standard deviation and the correlation coefficients of the data by

$$\sigma^{\rm data}_a(\boldsymbol{\Delta}) = \sigma\langle \tau_a(\boldsymbol{x}_1,\ \boldsymbol{x}_1 + \boldsymbol{\Delta})\rangle, \quad (17)$$

$$\mathrm{Cor}^{\rm data}_{a,b}(\boldsymbol{d},\ \boldsymbol{\Delta},\ \boldsymbol{\Delta}') = \mathrm{Cor}\left\langle \tau_a(\boldsymbol{x}_1,\ \boldsymbol{x}_2),\ \tau_b(\boldsymbol{x}'_1,\ \boldsymbol{x}'_2)\right\rangle, \quad (18)$$

in accordance with the definitions of equations (14) and (15).

In the case of point-to-annulus travel-time measurements, we consider two annuli with centers at coordinates $\boldsymbol{x}$ and $\boldsymbol{x}'$ and radii Δ and Δ', as depicted in Figure 4*b*. We estimate the covariance, standard deviation, and correlation coefficients by spatial averaging at fixed $\boldsymbol{d} = \boldsymbol{x}' - \boldsymbol{x}$, Δ, and Δ'. We use the following notation:

$$\mathrm{Cov}^{\rm data}_{\alpha,\beta}(\boldsymbol{d},\ \Delta,\ \Delta') = \mathrm{Cov}\left\langle \tau_\alpha(\boldsymbol{x};\ \Delta),\ \tau_\beta(\boldsymbol{x}';\ \Delta')\right\rangle, \quad (19)$$

$$\sigma^{\rm data}_\alpha(\Delta) = \sigma\langle \tau_\alpha(\boldsymbol{x};\ \Delta)\rangle, \quad (20)$$

$$\mathrm{Cor}^{\rm data}_{\alpha,\beta}(\boldsymbol{d},\ \Delta,\ \Delta') = \mathrm{Cor}\left\langle \tau_\alpha(\boldsymbol{x};\ \Delta),\ \tau_\beta(\boldsymbol{x}';\ \Delta')\right\rangle, \quad (21)$$

where the indices α and β refer to the type of travel times (either in, out, oi, or mn). Remember that all these quantities are functions of the duration of the observation, T.

Throughout this paper we use data from the *SOHO* MDI experiment (Scherrer et al. 1995). We consider a 35 hr long time series of high-resolution Dopplergrams obtained in 2001 May at a cadence of $h_t = 1$ minute. A region of area $L^2 = (250\ \mathrm{Mm})^2$ centered at 13° latitude, devoid of sunspots or plage, was tracked at the Carrington rate and interpolated onto Postel's azimuthal equidistant projection using the standard MDI pipeline processing. The spatial sampling is 0.068 heliocentric degrees ($h_x = 0.83$ Mm) or twice the original high-resolution pixel size at disk center. Better spatial sampling is unnecessary, as is shown in § 5. We split the data into 16 consecutive intervals of 128 minute length. We filter the data cubes using one of two types of filters: either an *f*-mode filter that removes all power away from the *f*-mode ridge (Fig. 1*a*)

or a Gaussian phase-speed filter for p-modes (Fig. 2a). We then measure both point-to-point and center-to-annulus travel times from the filtered data for each 128 minute segment using the procedures described in § 2. For $T = 128$ minutes, we then estimate the travel-time covariance functions by spatial averaging (we also average over all 16 segments to further improve the measurements). The observations are presented in §§ 5 and 6 and compared with the model developed in § 4.

4. A SIMPLE MODEL FOR THE NOISE COVARIANCE

4.1. *Assumptions of the Model*

Motivated by studies of realization noise for global helioseismology (e.g., Libbrecht 1992; Toutain & Appourchaux 1994), we begin by modeling the statistical properties of the discrete Fourier transform of the signal, $\phi(\boldsymbol{k}, \omega)$, where $\boldsymbol{k}$ is the horizontal wavevector and ω is the temporal angular frequency. For an observation of duration T and square area L^2, the discrete Fourier transform is given on a grid with increments of size $h_k = 2\pi/L$ for wavenumbers and $h_\omega = 2\pi/T$ for the angular frequency (Appendix A).

Let us denote by $\Psi(\boldsymbol{x}, t)$ the physical wave field on the surface of the Sun (for instance, the line-of-sight Eulerian velocity). The observed wave field is obtained by multiplication of $\Psi(\boldsymbol{x}, t)$ with a window function $W(\boldsymbol{x}, t)$, equal to 1 when data are available and 0 otherwise. In the Fourier domain, the filtered observable, $\phi(\boldsymbol{k}, \omega)$, is given by

$$\phi(\boldsymbol{k},\ \omega) = F(\boldsymbol{k},\ \omega)[\Psi * W](\boldsymbol{k},\ \omega), \tag{22}$$

where the asterisk is the three-dimensional convolution operation and $F(\boldsymbol{k}, \omega)$ is the analysis filter. The application of a window function has two effects. The window function induces correlations in the Fourier domain and smears the power over a volume of size $\sim h_k^2 h_\omega$. Note that for short observation times T, the temporal window function can cause significant broadening of the spectrum. In the absence of perturbations (e.g., no temperature variations and no flows), it is reasonable to assume that $\Psi(\boldsymbol{x}, t)$ is statistically spatially homogeneous and stationary in time, which implies that $E[\Psi(\boldsymbol{x}, t)\Psi(\boldsymbol{x}', t')]$ is only a function of $\boldsymbol{x} - \boldsymbol{x}'$ and $t - t'$. In Fourier space, this means that the $\Psi(\boldsymbol{k}, \omega)$ are uncorrelated, except that $\Psi^*(\boldsymbol{k}, \omega) = \Psi(-\boldsymbol{k}, -\omega)$, as $\Psi(\boldsymbol{x}, t)$ is real.

The simple noise model that we use in this paper assumes that there are no correlations between the values $\phi(\boldsymbol{k}, \omega)$ at distinct grid points (recall that the grid spacing is given by h_k and h_ω). We ignore the correlations introduced by convolution with the window function; these correlations are small when the spectrum of Ψ is smooth on the scales of h_k and h_ω. A necessary condition for this to be valid is that the typical damping time of the waves is less than T, so that the line width is larger than h_ω. At each point $(\boldsymbol{k}, \omega)$ in the Fourier grid, we model the observable as

$$\phi(\boldsymbol{k},\ \omega) = \sqrt{\mathcal{P}(\boldsymbol{k},\ \omega)}\mathcal{N}(\boldsymbol{k},\ \omega), \tag{23}$$

where $\mathcal{N}$ is a complex Gaussian random variable with independent real and imaginary parts, zero mean, and unit standard deviation ($E[\mathcal{N}\mathcal{N}^*] = 1$). The random variables $\mathcal{N}(\boldsymbol{k}, \omega)$ are uncorrelated except for the constraint $\mathcal{N}^*(\boldsymbol{k},\ \omega) = \mathcal{N}(-\boldsymbol{k},\ -\omega)$, which ensures that $\phi(\boldsymbol{x}, t)$ is real. One can invoke the central limit theorem to justify employing normal probability density functions. The expectation value of the power spectrum, i.e., the variance of $\phi(\boldsymbol{k}, \omega)$, is denoted by $\mathcal{P}(\boldsymbol{k}, \omega)$.

It is not straightforward to compute the expectation value of the power spectrum $\mathcal{P}(\boldsymbol{k}, \omega)$ from first principles; however, it is possible (Birch et al. 2004). Here we estimate $\mathcal{P}(\boldsymbol{k}, \omega)$ directly from the data. For example, for $T = 128$ minutes and $L = 250$ Mm, we consider 16 consecutive 128 minute quiet-Sun MDI data sets, compute their power spectra, and then compute the average of these spectra. The resulting average power spectrum, obtained on the grid with $h_\omega/2\pi = 1/T = 130.2$ μHz and $Rh_k = 2\pi R/L = 17.5$, is smooth and can be used as an estimate for the expectation value ($R = 696$ Mm is the solar radius). Remember that for each choice of T and L there are corresponding grid spacings in Fourier space. In addition, $\mathcal{P}(\boldsymbol{k}, \omega)$ depends on T and L through the effect of the temporal and spatial window functions.

We have now specified the procedure to compute a single realization of the observable for particular values of T and L (eq. [23]). In order to estimate the correlations between various travel-time measurements, we consider many realizations of the observable and measure the travel times for each. By averaging over many realizations we can estimate the travel-time covariance that results purely from realization noise. This approach is identical to the one used in global helioseismology (e.g., Toutain & Appourchaux 1994). Modeling the Fourier spectrum as consisting of independent bins and Gaussian complex random variables is the simplest approach that can be used. The ultimate justification of the model will, however, be its efficacy in explaining the observed data.

4.2. *Point-to-Point Travel Times*

For the case of point-to-point travel times, we can compute analytically the average of products of travel times over an infinity of realizations, i.e., take the expectation value. Given two complex random variables X and Y, the covariance $\mathrm{Cov}[X, Y]$, standard deviation $\sigma[X]$, and correlation coefficient $\mathrm{Cor}[X, Y]$ are defined by

$$\mathrm{Cov}[X,\ Y] = E[XY^*] - E[X]E[Y^*], \tag{24}$$

$$\sigma[X] = \sqrt{\mathrm{Cov}[X,\ X]}, \tag{25}$$

$$\mathrm{Cor}[X,\ Y] = \mathrm{Cov}[X,\ Y]/(\sigma[X]\sigma[Y]), \tag{26}$$

where E takes the expectation value (ensemble average).

For point-to-point travel times, we use again the geometry depicted in Figure 4a. The noise covariance of the travel times estimated by averaging over realizations we denote by

$$\mathrm{Cov}^{\mathrm{noise}}_{a,b}(\boldsymbol{d},\ \boldsymbol{\Delta},\ \boldsymbol{\Delta}') = \mathrm{Cov}\big[\tau_a(\boldsymbol{x}_1,\ \boldsymbol{x}_2),\ \tau_b\big(\boldsymbol{x}_1',\ \boldsymbol{x}_2'\big)\big]. \tag{27}$$

In the model, the covariance is translation invariant and thus depends only on the difference $\boldsymbol{d} = \boldsymbol{x}_1' - \boldsymbol{x}_1$, the vectors $\boldsymbol{\Delta} = \boldsymbol{x}_2 - \boldsymbol{x}_1$ and $\boldsymbol{\Delta}' = \boldsymbol{x}_2' - \boldsymbol{x}_1'$, and the duration of the observation T. As described in § 2, indices a and b refer to either +, −, mean, or diff.

In Appendix C we derive the following result:

$$\begin{aligned}\mathrm{Cov}^{\mathrm{noise}}_{a,b} = \frac{(2\pi)^3}{T}\ h_\omega \sum_\omega W_a^*(\boldsymbol{\Delta},\ \omega)\\ \times\big[W_b(\boldsymbol{\Delta}',\ \omega)\mathcal{C}(\boldsymbol{d},\ \omega)\mathcal{C}\big(\boldsymbol{x}_2 - \boldsymbol{x}_2',\ \omega\big)\big]\\ + \big[W_b^*(\boldsymbol{\Delta}',\ \omega)\mathcal{C}\big(\boldsymbol{x}_2' - \boldsymbol{x}_1,\ \omega\big)\mathcal{C}\big(\boldsymbol{x}_2 - \boldsymbol{x}_1',\ \omega\big)\big].\end{aligned} \tag{28}$$

In this expression, $W_a(\mathbf{\Delta}, \omega)$ is the temporal Fourier transform of $W_a(\mathbf{\Delta}, t)$. Recall that the travel times $\tau_a(\boldsymbol{x}_1, \boldsymbol{x}_2)$ are obtained from the cross-covariance function $C(\boldsymbol{x}_1, \boldsymbol{x}_2, t)$ through the appropriate weight functions $W_a(\mathbf{\Delta}, t)$. For example, for $a =$ diff, we have $W_{\rm diff} = W_+ - W_-$, where $W_\pm$ are defined in equation (4). In equation (28), the function $\mathcal{C}(\mathbf{\Delta}, \omega)$ is the expectation value of the cross-covariance function, obtained by taking the inverse spatial Fourier transform of the expected power spectrum:

$$\mathcal{C}(\boldsymbol{r}, \omega) = h_k^2 \sum_{\boldsymbol{k}} h_\omega h_k^2 \mathcal{P}(\boldsymbol{k}, \omega) e^{i\boldsymbol{k}\cdot\boldsymbol{r}}, \tag{29}$$

with

$$\mathcal{P}(\boldsymbol{k}, \omega) = E\left[|\phi(\boldsymbol{k}, \omega)|^2\right]. \tag{30}$$

Equation (28) shows that the dominant T-dependence of the covariance is like $1/T$ (there is a small effect from the temporal window function through $\mathcal{P}$). Otherwise, it depends only on the power spectrum $\mathcal{P}(\boldsymbol{k}, \omega)$ and the weight functions W_a and W_b. Evaluating equation (28) is more efficient computationally than performing a large number of Monte Carlo simulations. Note that we can easily obtain the correlation function $\mathrm{Cor}^{\rm noise}_{a,b}$ and the standard deviation $\sigma^{\rm noise}_a$ from $\mathrm{Cov}^{\rm noise}_{a,b}$.

4.3. *Center-to-Annulus Travel Times*

Equation (28) can be averaged over all the pairs of points that contribute to the center-to-annulus travel times. For the case in which $\mathcal{P}(\boldsymbol{k}, \omega)$ does not depend on the direction of $\boldsymbol{k}$, we can obtain an analytical approximation to the noise covariance $\mathrm{Cov}^{\rm noise}_{\alpha,\beta}(\boldsymbol{d}, \mathbf{\Delta}, \mathbf{\Delta}')$, as shown in Appendix D.2. This approximate result, equation (D6), is useful, as it gives insight into the somewhat complicated behavior of the covariance. However, to evaluate the noise model exactly, we perform Monte Carlo simulations. We generate realizations of the observable ϕ using the assumptions of the noise model described in § 4.1. We then measure center-to-annulus travel times from each realization and then compute the statistical properties of the travel times. The results of the Monte Carlo simulations are shown in § 5.2.

5. COMPARISON OF DATA AND MODEL

5.1. *Point-to-Point Travel Times*

Figure 5*a* shows the standard deviation in point-to-point *f*-mode travel-time measurements from the data and the model for $T = 128$ minutes. The filtered power spectrum is shown in Figure 1*a*; the dominant wavelength is about $\lambda = 5$ Mm. We look at the case in which $\mathbf{\Delta} = \Delta\hat{\boldsymbol{x}}$, i.e., the vector $\boldsymbol{x}_2 - \boldsymbol{x}_1$ points west. For $T = 128$ minutes, the data are completely dominated by realization noise, and the noise model (§ 4.1) accurately describes the standard deviation of the data. In Appendix D.1 we show that the standard deviation of $\tau_{\rm diff}$ approximately scales with distance Δ according to

$$\sigma_{\rm diff}(\Delta) \propto \sqrt{\Delta} \exp\left(\omega_0 \Gamma \Delta / g\right), \tag{31}$$

where ω_0 is the dominant frequency of the *f*-modes, Γ is the FWHM of the *f*-mode ridge around ω_0, and g is the gravitational acceleration at the solar surface. The increase of the standard deviation with distance is due to the combination of geometrical spreading ($\sqrt{\Delta}$ factor) and wave damping (exponential factor). We also note that the standard deviation

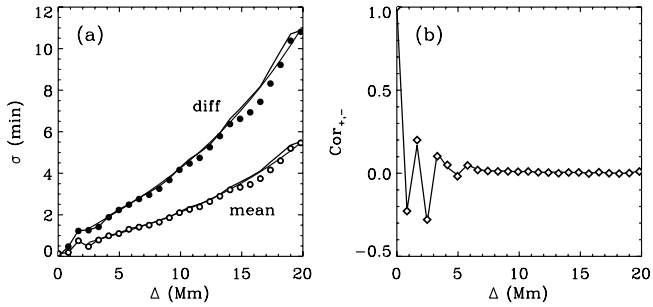

FIG. 5.—(*a*) Standard deviations $\sigma_{\rm diff}$ and $\sigma_{\rm mean}$ of the *f*-mode point-to-point travel times as a function of distance Δ. The observation time is $T =$ 128 minutes. The standard deviations from the data (*circles*) and from the noise model (*thick lines*) are shown. The thin lines show the far-field approximation from Appendix D.1. (*b*) Correlation between τ_+ and τ_- from the data (*diamonds*) and from the noise model (*solid line*).

$\sigma_{\rm diff}(\Delta)$ is larger than $\sigma_{\rm mean}(\Delta)$ by a factor of 2, except for when $\Delta < \lambda$. This can be understood by writing the ratio $\sigma_{\rm diff}/\sigma_{\rm mean}$ in terms of the correlation $\mathrm{Cor}_{+,-}$ between τ_+ and τ_-:

$$\frac{\sigma_{\rm diff}}{\sigma_{\rm mean}} = 2\sqrt{\frac{1 - \mathrm{Cor}_{+,-}}{1 + \mathrm{Cor}_{+,-}}}\,. \tag{32}$$

Since waves propagating in different directions are uncorrelated in the absence of solar perturbations, $\mathrm{Cor}_{+,-} \simeq 0$ for $\Delta > \lambda$ (Fig. 5*b*), and thus $\sigma_{\rm diff}/\sigma_{\rm mean} \simeq 2$. In the near field, $\mathrm{Cor}_{+,-}$ oscillates as a function of Δ around 0 with a period of roughly $\lambda/2$.

Figure 6 shows the correlations $\mathrm{Cor}_{a,b}(\boldsymbol{d})$ of the point-to-point *f*-mode travel times as a function of $\boldsymbol{d} = (d_x, d_y)$ at fixed $\mathbf{\Delta} = \mathbf{\Delta}' = (10\ \mathrm{Mm})\hat{\boldsymbol{x}}$ and $T = 128$ Mm, for both the data and the noise model. The plots show the cases of $a = b =$ diff, $a = b =$ mean, and the cross term $(a, b) =$ (mean, diff). The correlation of the cross-term is always less than 0.1 in absolute value; this correlation would be exactly 0 if the power spectrum were isotropic. The correlations $\mathrm{Cor}_{a,a}(\boldsymbol{d})$, where $a =$ mean or diff, look similar and fall off very rapidly with $d = \|\boldsymbol{d}\|$; they both have a central peak with a FWHM of $l = 2.5$ Mm. Since the central wavelength of the *f*-mode power spectrum is $\lambda \simeq 5$ Mm, the correlation length is $l \simeq \lambda/2$. The spatial sampling of the filtered wave field is sufficient, as the pixel size is less than $l/2$. The correlation peak has a sidelobe with amplitude of about 0.1 at distance 2.5 Mm away from $\boldsymbol{d} = 0$. The correlation maps display an anisotropic component due to the instrumental modulation transfer function (MTF) (astigmatism) and line-of-sight projection effects (power depends on the direction of $\boldsymbol{k}$); this is taken into account in the noise model. Most of the fine details in the correlations are accurately reproduced by the noise model, in particular, near $\boldsymbol{d} = \pm\mathbf{\Delta}$, i.e., where $\boldsymbol{x}_1' = \boldsymbol{x}_2$ or $\boldsymbol{x}_2' = \boldsymbol{x}_1$.

Rather than computing the covariance $\mathrm{Cov}_{a,a}(\boldsymbol{d})$ by explicit spatial averaging (§ 3 and eq. [12]), we can obtain the covariance by inverse Fourier transformation of the power spectrum of the travel maps $\tau_a(\boldsymbol{x}_1, \boldsymbol{x}_2)$ at fixed $\mathbf{\Delta}$. It can be shown that

$$\mathrm{Cov}_{a,a}(\boldsymbol{d}) = h_k^2 \sum_{\boldsymbol{k}} |\tau_a(\boldsymbol{k})|^2 e^{i\boldsymbol{k}\cdot\boldsymbol{d}}, \tag{33}$$

where $\tau_a(\boldsymbol{k})$ is the inverse Fourier transform of $\tau_a(\boldsymbol{x}_1, \boldsymbol{x}_1 + \mathbf{\Delta})$ with respect to the point $\boldsymbol{x}_1$:

$$\tau_a(\boldsymbol{k}) = \frac{h_x^2}{(2\pi)^2} \sum_{\boldsymbol{x}_1} \tau_a(\boldsymbol{x}_1, \boldsymbol{x}_1 + \mathbf{\Delta}) e^{-i\boldsymbol{k}\cdot\boldsymbol{x}_1}. \tag{34}$$

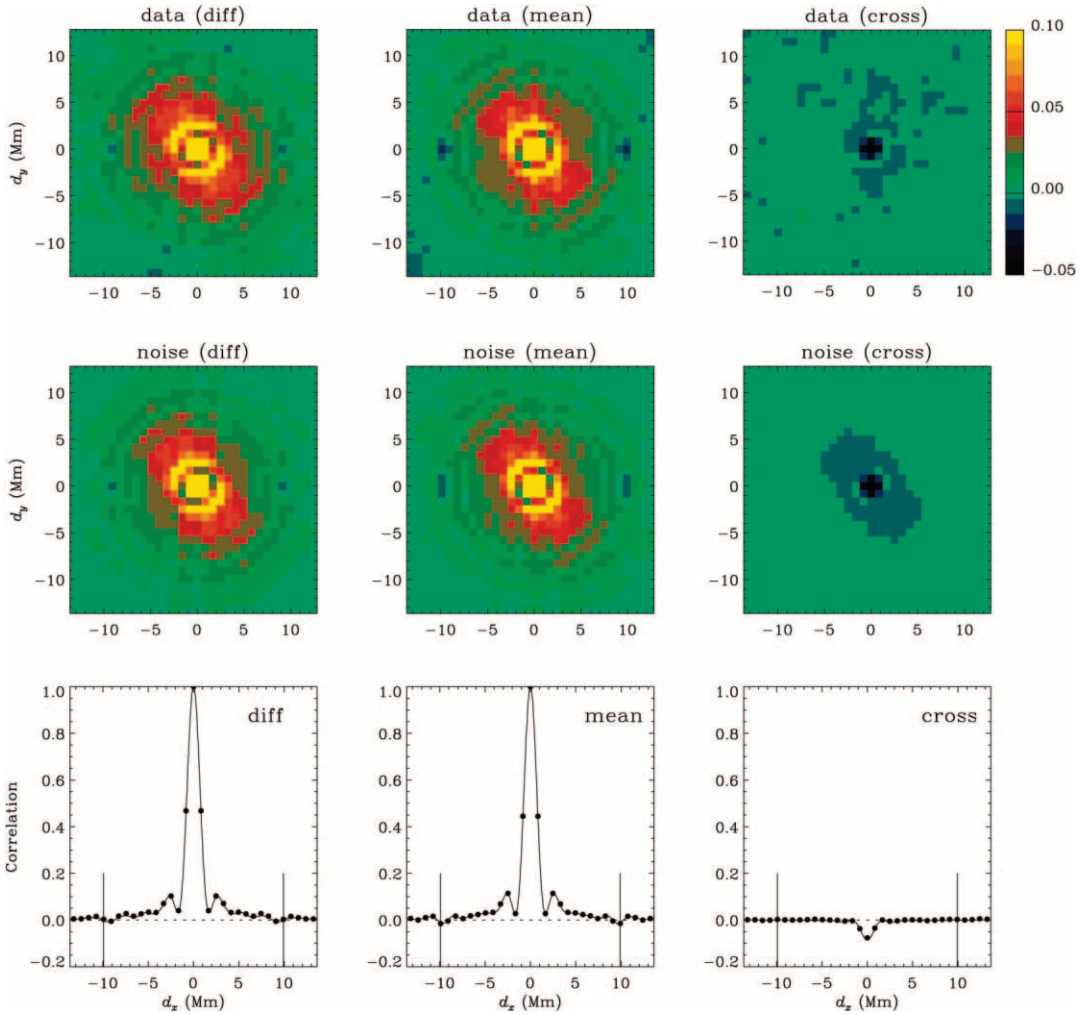

FIG. 6.—Correlation plots for *f*-mode point-to-point travel times. The top row of panels shows the data correlations $\mathrm{Cor}^{\mathrm{data}}_{a,b}(\boldsymbol{d})$ as functions of $\boldsymbol{d} = (d_x,\ d_y)$ at fixed $\boldsymbol{\Delta} = \boldsymbol{\Delta}' = (10\ \mathrm{Mm})\hat{\boldsymbol{x}}$ and $T = 128$ Mm (see § 3, Fig. 4*a*). The left column is for $a = b =$ diff, the middle column is for $a = b =$ mean, and the right column is for the cross-term $(a,\ b) =$ (mean, diff). The color scale is restricted to the range $[-0.05, 0.1]$ to show details. The middle row of panels shows the corresponding noise correlations $\mathrm{Cor}^{\mathrm{noise}}_{a,b}(\boldsymbol{d})$ estimated from the model described in § 4.1. The bottom row of panels shows slices at $d_y = 0$ through the travel-time correlation matrices as functions of d_x. In these plots, the circles show the data, and the solid curves show the noise model.

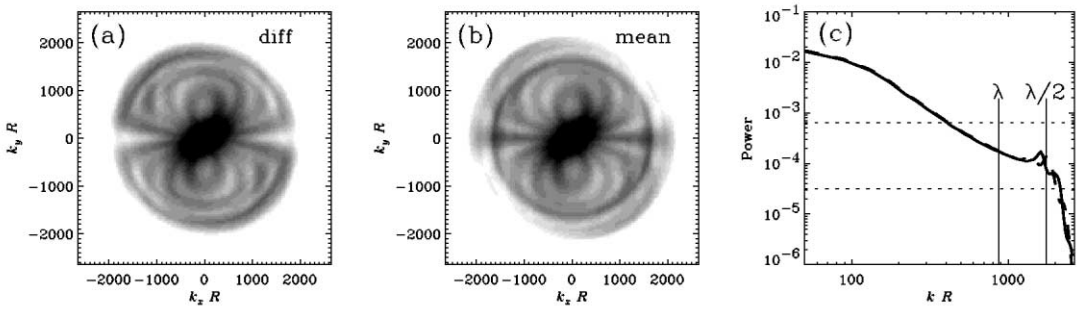

FIG. 7.—Spatial power spectra of the point-to-point travel-time maps τ_{diff} and τ_{mean} at fixed $\boldsymbol{\Delta} = (10\ \mathrm{Mm})\hat{\boldsymbol{x}}$. The travel times are measured using the *f*-mode filter and $T = 128$ minutes. The power $S_a(\boldsymbol{k}) = |\tau_a(\boldsymbol{k})|^2$ is equivalent to the Fourier transform of the covariance map $\mathrm{Cov}_{a,a}(\boldsymbol{d})$ shown in Fig. 6. (*a*) Power $S_{\mathrm{diff}}(\boldsymbol{k})$ as a function of wavevector $\boldsymbol{k} = (k_x,\ k_y)$. The spatial Nyquist frequency is at $kR = 2600$. The gray scale is logarithmic and covers the range between the two dashed lines shown in (*c*). (*b*) Power $S_{\mathrm{mean}}(\boldsymbol{k})$. (*c*) Azimuthal average of $S_{\mathrm{diff}}(\boldsymbol{k})$ (*solid line*) and the azimuthal average of $S_{\mathrm{mean}}(\boldsymbol{k})$ (*thick dashed line*) vs. $k = \| \boldsymbol{k} \|$. The vertical lines show the values of k corresponding to the wavelengths λ and $\lambda/2$, where $\lambda = 5$ Mm for the *f*-mode case.

The power spectra $S_a(\boldsymbol{k}) = |\tau_a(\boldsymbol{k})|^2$ for observed *f*-mode travel times are plotted in Figure 7 for both $a =$ diff and $a =$ mean at $\Delta = 10$ Mm. Such plots were first studied by T. L. Duvall, Jr. (2002, private communication). According to equation (33) the power $S_a(\boldsymbol{k})$ is the Fourier transform of the covariance map $\mathrm{Cov}_{a,a}(\boldsymbol{d})$ shown in Figure 6. We see that there is a critical wavenumber k_c beyond which the power drops precipitously. This cutoff occurs at $k_c \simeq 4\pi/\lambda$ (see Appendix E). This is consistent with a correlation length $l \simeq \lambda/2$, as seen in the correlation maps (Fig. 6). There are noticeable differences

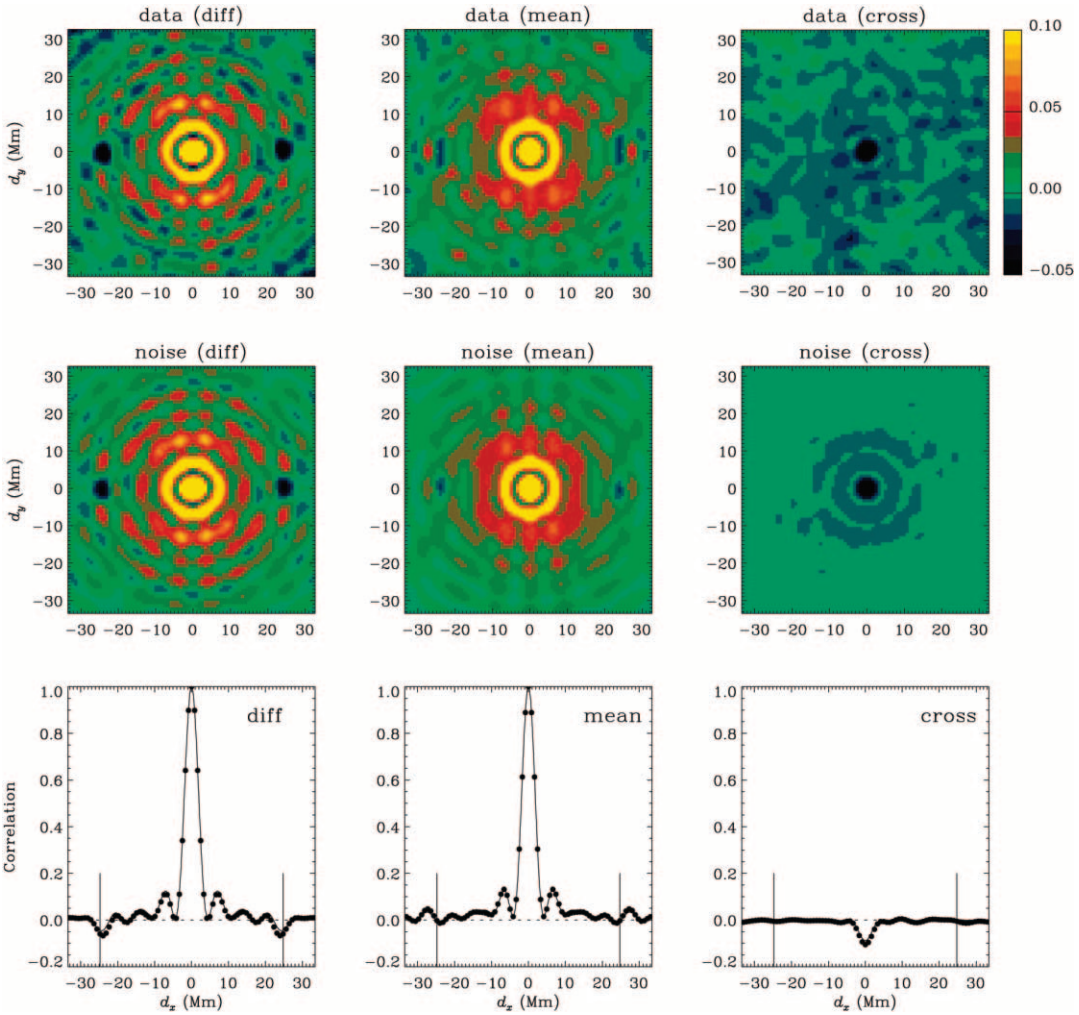

FIG. 8.—Correlation plots for p-mode point-to-point travel times. The top row of panels shows the data correlations $\mathrm{Cor}^{\mathrm{data}}_{a,b}(\boldsymbol{d})$ as functions of $\boldsymbol{d} = (d_x,\ d_y)$ at fixed $\boldsymbol{\Delta} = \boldsymbol{\Delta}' = (25\ \mathrm{Mm})\hat{\boldsymbol{x}}$ and $T = 128$ Mm (see § 3, Fig. 4*a*). The left column is for $a = b =$ diff, the middle column is for $a = b =$ mean, and the right column is for the cross-term $(a,\ b) =$ (mean, diff). The color scale is restricted to the range $[-0.05, 0.1]$ to show details. The middle row of panels shows the corresponding noise correlations $\mathrm{Cor}^{\mathrm{noise}}_{a,b}(\boldsymbol{d})$ estimated from the model described in § 4.1. The bottom row of panels shows slices at $d_y = 0$ through the travel-time correlation matrices as functions of d_x. In these plots, the circles show the data, and the solid curves show the noise model.

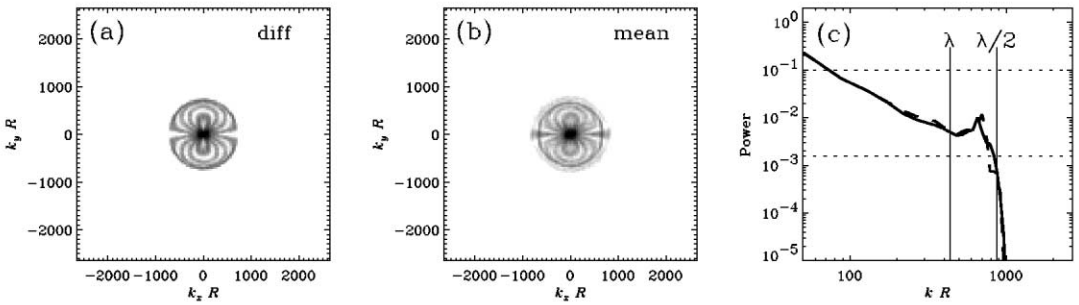

FIG. 9.—Spatial power spectra of the point-to-point travel-time maps τ_{diff} and τ_{mean} at fixed $\boldsymbol{\Delta} = (25\ \mathrm{Mm})\hat{\boldsymbol{x}}$. The travel times are measured using the p-mode filter and $T = 128$ minutes. The power $S_a(\boldsymbol{k}) = |\tau_a(\boldsymbol{k})|^2$ is equivalent to the Fourier transform of the covariance map $\mathrm{Cov}_{a,a}(\boldsymbol{d})$ shown in Fig. 8. (*a*) Power $S_{\mathrm{diff}}(\boldsymbol{k})$ as a function of wavevector $\boldsymbol{k} = (k_x,\ k_y)$. The spatial Nyquist frequency is at $kR = 2600$. The gray scale is logarithmic and covers the range between the two dashed lines shown in (*c*). (*b*) Power $S_{\mathrm{mean}}(\boldsymbol{k})$. (*c*) Azimuthal average of $S_{\mathrm{diff}}(\boldsymbol{k})$ (*thick solid line*) and the azimuthal average of $S_{\mathrm{mean}}(\boldsymbol{k})$ (*thick dashed line*) vs. $k = \| \boldsymbol{k} \|$. The vertical lines show the values of k corresponding to the wavelengths λ and $\lambda/2$, where $\lambda = 10$ Mm for the p-mode case.

between the spatial power maps $S_{\mathrm{diff}}(\boldsymbol{k})$ and $S_{\mathrm{mean}}(\boldsymbol{k})$, in particular, along the line $k_y = 0$. For short T, most of these details, which come directly from the shape of the filtered power spectrum $\mathcal{P}(\boldsymbol{k}, \omega)$ of the wave field, can be reproduced by the noise model from § 4.1 and equation (33). The contribution from supergranulation at $kR \sim 120$ can hardly be seen in point-to-point travel times: it becomes more obvious in center-to-annulus travel times (§ 5.2).

Figure 8 shows the data and the model of the covariance of the point-to-point travel times, $\mathrm{Cor}_{a,b}(\boldsymbol{d})$, in the case of the

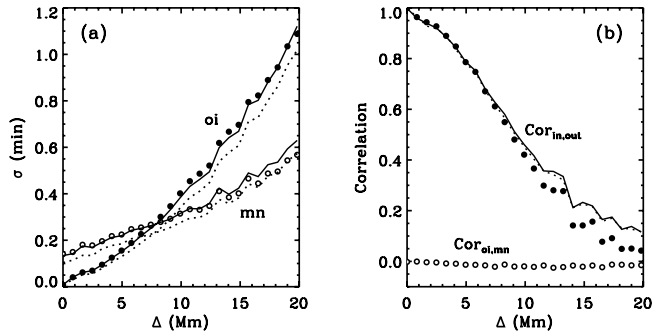

FIG. 10.—(*a*) Standard deviations, $\sigma_{\rm oi}$ and $\sigma_{\rm mn}$, for the *f*-mode center-to-annulus travel times as a function of annular radius Δ. The standard deviations from the data (*circles*) and from the noise model (*thick lines*) are shown. The dotted lines show the approximation from Appendix D.2. The observation time is $T = 128$ minutes. (*b*) Correlation $\mathrm{Cor}_{\rm in,\,out}$ between $\tau_{\rm out}$ and $\tau_{\rm in}$ from the data (*filled circles*), the noise model (*solid line*), and the approximation (*dotted line*). The open circles show the correlation $\mathrm{Cor}_{\rm oi,\,mn}$ between $\tau_{\rm oi}$ and $\tau_{\rm mn}$ from the data.

p-mode filter shown in Figure 2*a*. The parameters are the same as in the *f*-mode case except for $\mathbf{\Delta} = \mathbf{\Delta}' = (25\ \mathrm{Mm})\hat{\boldsymbol{x}}$. The width l of the central peak is larger than in the *f*-mode case because the dominant wavelength of the filtered *p*-mode power is about $\lambda = 10$ Mm. The relation $l \simeq \lambda/2$ remains valid for the *p*-mode example. The power spectra $S_a(\boldsymbol{k})$ for the *p*-mode case are shown in Figure 9, and again the critical wavenumber is given by $k_c \simeq 4\pi/\lambda$.

5.2. *Center-to-Annulus Travel Times*

Figure 10*a* shows the standard deviations, $\sigma_{\rm oi}$ and $\sigma_{\rm mn}$, for the *f*-mode center-to-annulus travel times as a function of annular radius Δ for $T = 128$ minutes. As T is small, the noise model is in close agreement with the data. For large distances Δ, we have $\sigma_{\rm oi}/\sigma_{\rm mn} \simeq 2$, as we saw before in the point-to-point case (§ 5.1). However, for distances $\Delta < 8$ Mm the standard deviation of the "oi" travel times is smaller than for the "mn" travel times. This counterintuitive result comes from the strong correlation $\mathrm{Cor}_{\rm out,\,in}$ between "in" and "out" travel times for small annuli (see Fig. 10*b*). As in the point-to-point case (eq. [32]) we can write

$$\frac{\sigma_{\rm oi}}{\sigma_{\rm mn}} = 2\sqrt{\frac{1-\mathrm{Cor}_{\rm out,\,in}}{1+\mathrm{Cor}_{\rm out,\,in}}}\,. \tag{35}$$

In particular, $\mathrm{Cor}_{\rm out,\,in} \to 1$ implies $\sigma_{\rm oi}/\sigma_{\rm mn} \to 0$. For very small Δ we have $\mathrm{Cor}_{\rm out,\,in} \to 1$, because the waves that converge toward the annulus center are the same waves that diverge from it. As Δ increases, the correlation $\mathrm{Cor}_{\rm out,\,in}$ tends to 0 because the waves that contribute to $\tau_{\rm in}$ (the waves that propagate from the annulus to the center) do not contribute to $\tau_{\rm out}$ if the damping distance $\Delta_{\rm damp}$ is less than the annular radius Δ. Note that $\sigma_{\rm oi} = \sigma_{\rm mn}$ when $\mathrm{Cor}_{\rm out,\,in} = \frac{3}{5}$. As seen in Figure 10*b*, the correlation $\mathrm{Cor}_{\rm oi,\,mn}$ is very small (≈ -0.02), implying that these travel times are nearly independent. This is additional motivation for doing data analysis with the "oi" and "mn" travel times rather than the one-way travel times; the "oi" and "mn" travel times were originally introduced by Duvall et al. (1996) as a means to distinguish wave-speed perturbations from mass flows.

Figure 11 shows the travel-time correlations $\mathrm{Cor}_{\rm oi,\,oi}$ and $\mathrm{Cor}_{\rm mn,\,mn}$ for concentric annuli with different radii, Δ and Δ'. Since the annuli are concentric ($\boldsymbol{d} = 0$), the correlation is 1 when $\Delta = \Delta'$. The correlation oscillates with $|\Delta - \Delta'|$, and the off-diagonal elements with the largest absolute values are on the sub- and superdiagonals with $|\Delta - \Delta'| < \lambda/2$. We note that there are matrix elements near the diagonal that have very strong anticorrelations ($\mathrm{Cor} < -0.5$). The correlation matrices are not sparse; a large fraction of the correlations are above 50% in absolute value, especially when both Δ and Δ' are large. The correlation remains large far from the diagonal $\Delta = \Delta'$. This may have important implications for the inversion of time-distance data (e.g., Gough 1996; Gough & Sekii 2002); current time-distance inversions do not take into account these correlations (e.g., Kosovichev 1996; Gizon et al. 2000; Jensen et al. 2001; Zhao et al. 2001).

For $T = 128$ minutes, the correlation matrices (Fig. 11) for the data and the noise model are remarkably similar for the "mn" travel times, indicating that the correlations in the observed "mn" travel times are not caused by wave-speed inhomogeneities. The cut at $\Delta' = 5$ Mm through the correlation of the "mn" times shows the detailed agreement between the data and the model in this case. However, there are noticeable differences between the correlation matrices for the "oi" travel times. Unlike in the "mn" case, the "oi" correlations are larger for the solar data than for the noise model: this is due to the supergranulation flows. The cut through the "oi" correlation maps clearly shows that the data are more correlated than predicted by the model.

Figures 12*a* and 12*b* show the travel-time correlations $\mathrm{Cor}_{\rm mn,mn}$ and $\mathrm{Cor}_{\rm oi,oi}$ for offset annuli with common radius $\Delta = \Delta' = 5$ Mm as a function of offset $d = \|\boldsymbol{d}\|$ (see Fig. 4*b* for the geometry). In these plots we consider the *f*-mode data with $T = 128$ minutes, as in Figure 11. The correlation coefficient for the "mn" and "oi" signals decreases with increasing d. As was seen in Figure 11, the "oi" travel times are more correlated in the data than in the noise model, while the data and the noise model give very similar results for the correlation of the "mn" times. In order to investigate the spatial scales that cause the excess correlation in the "oi" travel times with respect to the noise prediction, we look at the power spectrum of the travel times. Figures 12*c* and 12*d* show the azimuthal average of the power spectra $S_{\rm mn}(\boldsymbol{k})$ and $S_{\rm oi}(\boldsymbol{k})$ of the travel-time maps for $\Delta = 5$ Mm; these can be constructed by taking the spatial Fourier transform of the functions $\mathrm{Cov}_{\rm mn,\,mn}(\boldsymbol{d})$ and $\mathrm{Cov}_{\rm oi,\,oi}(\boldsymbol{d})$. For $kR > 300$ the data and the noise model agree well, i.e., the spatial variations in the travel times at wavelengths less than $\sim$15 Mm are mostly due to realization noise (remember that $\lambda \simeq \Delta = 5$ Mm and $T = 128$ minutes). The log-log plot of the "mn" power spectrum (Fig. 12*c*) was first observed by Jensen et al. (2003). In Figures 12*d* and 12*f* we detect a solar signal in the "oi" travel times that peaks around $kR \simeq 120$, corresponding to the dominant wavenumber of supergranular flows seen in the direct Doppler data (Hathaway et al. 2000) and other time-distance studies (Duvall & Gizon 2000). This excess power with respect to the noise background demonstrates that we are able to measure the solar signal for an observation time as short as 2 hr. Note that for the "oi" travel times the background noise computed from the model is not a monotonic function of k but has a local maximum at $kR \simeq 160$. The cutoff of the power at a wavelength near $\lambda/2$ is seen again, as in the point-to-point case (§ 5.1). In Figures 12*c* and 12*e* there is also some evidence of excess power in the "mn" travel times around $kR \simeq 120$, but the main contribution is from the lowest wavenumbers. These slowly varying field effects are likely caused by line-of-sight

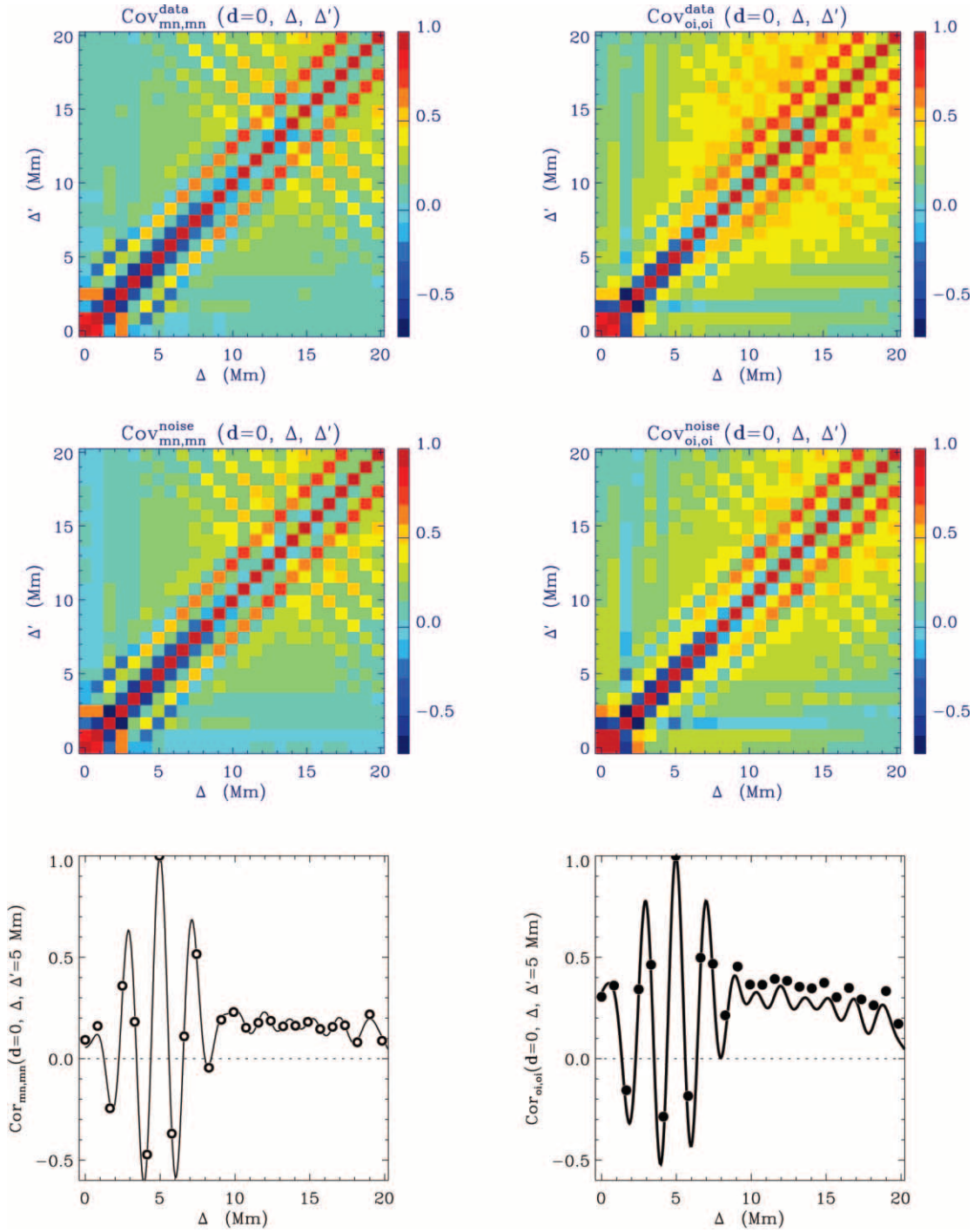

FIG. 11.—Correlations Cor($\boldsymbol{d} = 0,\ \Delta,\ \Delta'$) between f-mode travel times for concentric annuli as a function of annular radii Δ and Δ' (see Fig. 4*b* for the geometry). The top row is for the measurements ($T = 128$ minutes), and the middle row is for the noise model. The correlations for the "mn" times are shown in the left column, and for the "oi" times in the right column. The panels in the bottom row show slices at $\Delta' = 5$ Mm. The circles show the observations, and the solid lines show the noise model. Note that the observed "oi" correlations are larger than the "oi" correlations in the noise model. This is due to a real solar signal (supergranulation), as discussed in § 5.2.

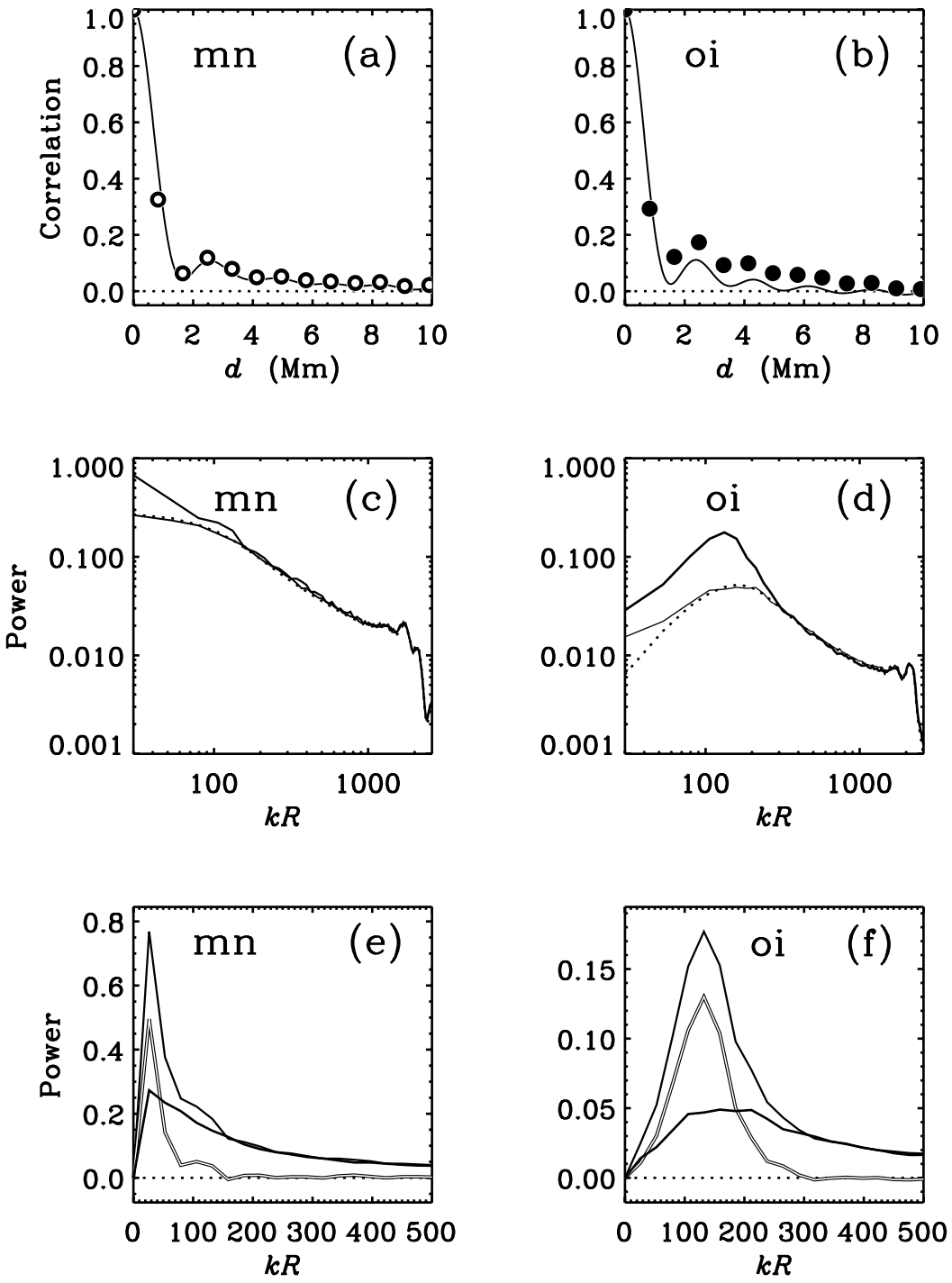

FIG. 12.—(*a*) Correlations $\mathrm{Cor}_{\mathrm{mn,mn}}(\boldsymbol{d}, \Delta, \Delta')$ between *f*-mode travel times for offset annuli with common radius $\Delta = \Delta' = 5$ Mm (see Fig. 4*b* for the geometry). The correlation has been averaged over the direction of the offset $\boldsymbol{d}$. The circles show the observations, and the solid lines show the noise model. The observation time is $T = 128$ minutes. (*b*) Correlations for the "oi" *f*-mode travel times. (*c*) Spatial power spectrum of the "mn" travel times at fixed $\Delta = 5$ Mm. The thick solid line shows the observations, and the thin solid line shows the noise model. The dotted line is for the approximation to the noise model. The Nyquist frequency is at $kR = 2600$. Both axes are logarithmic. (*d*) Spatial power spectrum of the "oi" travel times at fixed $\Delta = 5$ Mm. The thick solid line shows the observations, and the thin solid line shows the noise model. The dotted line is for the approximation to the noise model. (*e*) Difference (*double thin line*) between the measured spatial power (*thick line*) and the noise background computed from the model (*thin line*) for the "mn" travel times. Note that the axes are linear rather than logarithmic. (*f*) Same as in (*e*) but for the "oi" travel times. The excess power around $kR = 120$ is due to supergranular flows.

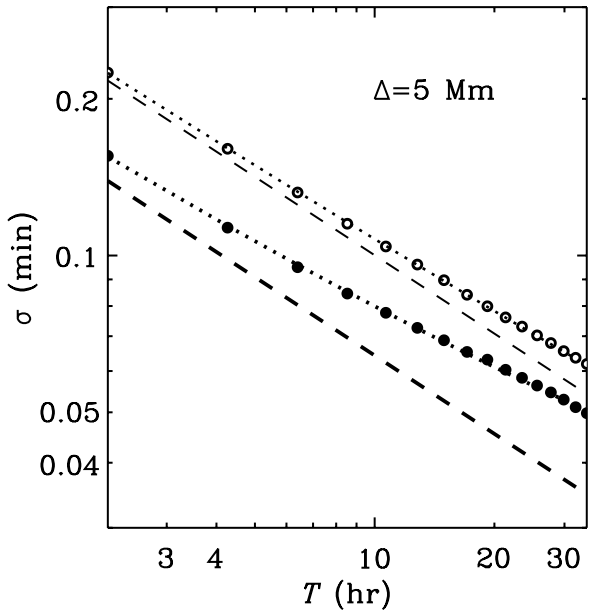

FIG. 13.—Standard deviations $\sigma^{\rm data}$ of the observed center-to-annulus f-mode travel times as functions of observation time T, on a log-log scale. The "oi" data are the filled circles, and the "mn" data are the open circles, both measured at $\Delta = 5$ Mm. The dotted lines are fits of the form $\sigma^{\rm fit} = NT^{-1/2} + S$ to the data over the interval 2 hr $< T <$ 35 hr, where N and S are free parameters. The dashed lines show the noise components $NT^{-1/2}$ from the fits.

projection effects and spatial variations in the point-spread function of the MDI telescope.

6. SIGNAL-TO-NOISE RATIO

In this section we study the signal-to-noise ratio in the travel-time maps as a function of observation duration T. Rather than relying on the noise model of § 4.1, we show that the noise can be estimated directly from the data by looking at the T-dependence of the standard deviation of the observed travel times.

We consider center-to-annulus f-mode travel times only. The thickness of the annulus is $w = 0.41$ Mm (see eqs. [7] and [8]). In our noise model, described in § 4.1, the standard deviation of the noise decreases as $T^{-1/2}$, as long as T is larger than the wave lifetimes. In Figure 13 we plot $\sigma^{\rm data}$ as a function of T for the "oi" and the "mn" travel times and $\Delta =$ 5 Mm. Any deviation from the $T^{-1/2}$ dependence must be due to the signal. In order to estimate the signal-to-noise ratio directly from the data, we fit the function $\sigma^{\rm fit} = NT^{-1/2} + S$ to $\sigma^{\rm data}$ over the interval 2 hr $< T <$ 35 hr, where N and S are positive constants determined by the fit. This model is the simplest possible model and is the result of adding a time-independent signal S to a noise background $NT^{-1/2}$. This fit works remarkably well, implying that the solar signal is mostly constant in time for $T <$ 35 hr. This is not too surprising, as the lifetime of the supergranulation pattern is larger than 1 day (the additional systematic effects that may be present are likely to be slowly varying in time as well). As was explained in § 5.2, the "oi" signal is dominated by supergranular flows.

Figure 14 shows the measured signal-to-noise ratio, defined by $r = T^{1/2}\sigma^{\rm data}/N - 1$, for the "oi" travel times as a function of both T and annular radius Δ. The signal-to-noise ratios that we measure for $T <$ 35 hr and $\Delta <$ 20 Mm do not exceed 1.1.

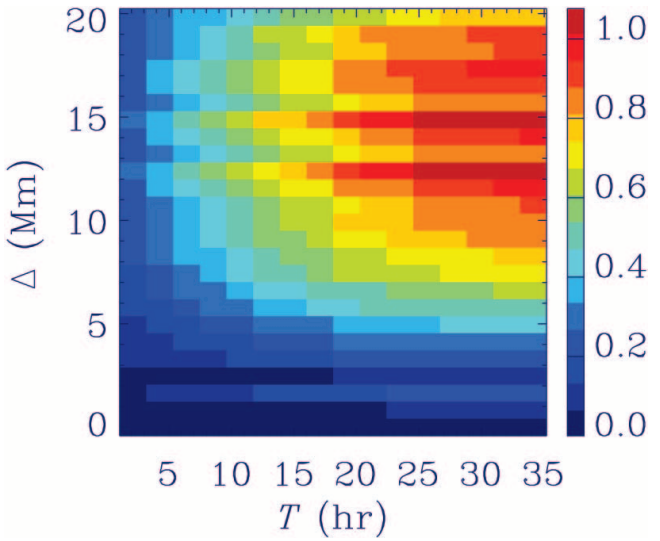

FIG. 14.—Signal-to-noise ratio estimated from the "oi" data, $r = T^{1/2}\sigma^{\rm data}/N - 1$, where N is obtained from fits of the type shown in Fig. 13.

The signal-to-noise ratio r is an increasing function of T for all distances Δ. This is consistent with the assumption that the signal is nearly time independent. At fixed T, r goes through a maximum at a distance near $\Delta = 12$ Mm. As expected, time-distance measurements of supergranular flows are most sensitive when the annular radius is roughly half the typical diameter of the supergranules (∼30 Mm). The signal-to-noise ratio can be increased well beyond 1 by averaging over a range of distances (Duvall et al. 1997; Duvall & Gizon 2000).

Figure 15 shows the signal-to-noise ratio for the "oi" and "mn" travel times, at fixed $\Delta = 5$ Mm. The time dependence of r (*solid line*) is close to the fit $T^{1/2}$(S/N) (*dashed line*). However, some small deviations occur for the "oi" travel times when $T >$ 15 hr, indicating that the solar signal is not quite constant in time. This is likely a result of the finite lifetime of solar supergranulation.

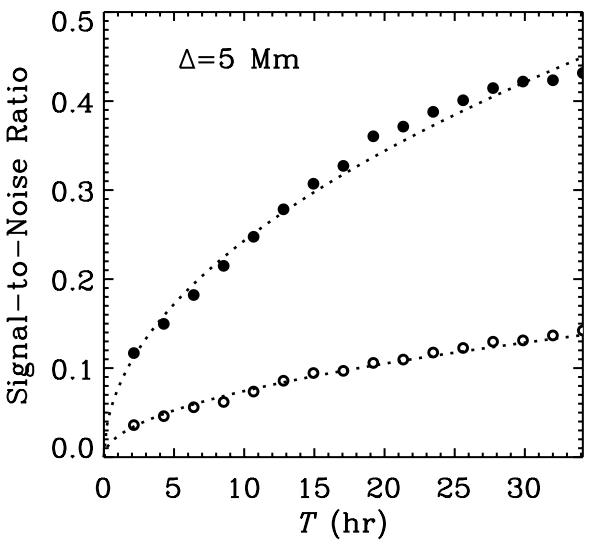

FIG. 15.—Signal-to-noise ratio as a function of observation time T for $\Delta = 5$ Mm. The filled circles show $r = T^{1/2}\sigma^{\rm data}/N - 1$ for the "oi" travel times, and the open circles show r for the "mn" travel times (cuts through Fig. 14). The dashed lines show the fits $T^{1/2}$(S/N).

7. DISCUSSION

We have introduced a new definition of travel time that allows the measurement of travel times for very noisy cross-covariances and reduces to the definition of Gizon & Birch (2002) in the limit of extensive spatial or temporal averaging. Comparison of the predictions from a simple model with noise estimates from *SOHO* MDI data have shown that the dominant noise source in time-distance travel times is realization noise. Our model for realization noise is valid for both p- and f-modes and for any spatial averaging scheme (point-to-point or center-to-annulus measurements, for example). The model is based on modeling the observed wave field as a complex uncorrelated Gaussian field in the Fourier domain.

From both the data and the model we show that the noise increases with the distance Δ, because of geometrical spreading and damping, and decreases with observation time T as $T^{-1/2}$. The noise is spatially correlated for both point-to-point and center-to-annulus measurements; in particular, the correlation remains large for measurements with the same central point but annuli of very different radii. The correlation length of the travel times is about $\lambda/2$, where λ is the dominant wavelength of the filtered wave field. The length scale $\lambda/2$ appears as a cutoff wavenumber $k_c = 4\pi/\lambda$ in the power spectrum of the travel times. Thus, there is little hope of detecting a solar signal at horizontal scales less than $\lambda/2$ from the travel times of wave packets with a dominant wavelength of λ. We estimate that with MDI high-resolution data, the ultimate horizontal spatial resolution that can be obtained through time-distance helioseismology near the surface can be no better than a few megameters.

Of course, the observed travel times are not entirely due to realization noise. Using the knowledge that realization noise scales as $T^{-1/2}$, we estimate the signal-to-noise ratio r for travel times as a function of annular radius Δ and observation time T. We see in quiet-Sun data that r increases with T and is maximum when Δ is about half the length scale of supergranulation. In the quiet Sun, r is larger for the "oi" travel times than for the "mn" travel times by about a factor of 3.

The central assumption in the noise model is in the form of the fourth moments of the wave field in the Fourier domain,

$$E[\phi(\boldsymbol{k}_1,\ \omega_1)\phi(\boldsymbol{k}_2,\ \omega_2)\phi(\boldsymbol{k}_3,\ \omega_3)\phi(\boldsymbol{k}_4,\ \omega_4)].$$

These moments can be calculated by assuming that the $\phi(\boldsymbol{k}, \omega)$ are uncorrelated on the Fourier grid and normally distributed. The same moments could be used to calculate the noise level of other types of local helioseismic measurements, for example, ring diagrams, acoustic holography, or Hankel analysis.

The noise covariance matrix for travel times is an important ingredient for inverting travel times, especially as we have shown that the noise covariance is far from diagonal. Accurate knowledge of the noise covariance will also allow the accurate assignment of error estimates to inversion results. We have seen that the power spectrum of travel times is strongly affected by noise and depends on the filtered power spectrum of the wave field. Our simple model for the noise covariance can be used to predict the noise level for various types of measurements, for example, for different filters (instrumental MTF or data analysis filters) or observation times T. This model may be useful in designing experiments to obtain travel time measurements with some desired noise level.

We expect that the noise model presented here will fail when the observation time T becomes so small that individual wave excitation events can be identified. In this limit the assumption that the Fourier components of the wave field are independent will fail, and as a result the noise predictions will not be accurate. However, this does not appear to be a major issue for routine time-distance work.

The definition of travel time that we introduced in this paper is certainly not the optimal definition. In particular, it does not take into account the statistics of the noise in the cross-covariance function. Realization noise in the time-domain cross-covariance is highly correlated, as the noise is mostly in the 3 mHz range. Travel-time fitting should presumably either take account of this correlation or be done in the frequency domain in which the noise in the cross-covariance at different frequencies is uncorrelated, although this does not remain true once nonsteady perturbations or flows are introduced (e.g., Woodard 2002; Woodard & Fan 2004). The travel-time measurement procedure developed in this paper needs to be extended before it can be applied to the study of sunspots or other strong perturbations. In particular, the fit should include other parameters such as the amplitude of the cross-covariance, since the assumption that the expectation value of the cross-covariance function is spatially uniform is clearly not valid near sunspots and active regions.

In future work we plan to study the inversion of time-distance data. With the completion of that work we will have a practical and self-consistent method for time-distance helioseismology, with the forward problem (Gizon & Birch 2002), the noise model (this paper), and the inverse problem all done within a physically motived and consistent model.

This work was supported by NASA grant NAG5-13261 to Stanford University. *SOHO* is a mission of international cooperation between the European Space Agency and NASA. We thank Tom Duvall for providing the tracked data cube that we used in this paper.

APPENDIX A

CONVENTIONS AND NOTATIONS

Let us consider a function $Q(\boldsymbol{x}, t)$ of discrete horizontal position $\boldsymbol{x}$ and discrete time t. We denote by h_x the sampling interval in the two spatial directions and by h_t the sampling interval in the time domain. The number of samples is $N_x = L/h_x$ in each spatial direction and $N = T/h_t$ in the time direction. For a centrally situated origin, $Q(\boldsymbol{x}, t)$ is evaluated on the grid $\boldsymbol{x}_{mn} = mh_x\hat{\boldsymbol{x}} + nh_x\hat{\boldsymbol{y}}$, where m and n are integers in the range $[-N_x/2,\ N_x/2 - 1]$, and $t_j = jh_t$, where j is an integer in the range $[-N/2,\ N/2 - 1]$. We employ the convention that the discrete Fourier transform of $Q(\boldsymbol{x}, t)$ is given by

$$Q(\boldsymbol{k},\ \omega) = \frac{h_x^2 h_t}{(2\pi)^3} \sum_{m,n,j} Q(\boldsymbol{x}_{mn},\ t_j) e^{-i\boldsymbol{k}\cdot\boldsymbol{x}_{mn} + i\omega t_j}. \tag{A1}$$

The horizontal wavevector $\boldsymbol{k}$ can take the discrete values $\boldsymbol{k}_{mn} = mh_k\hat{\boldsymbol{x}} + nh_k\hat{\boldsymbol{y}}$, where $h_k = 2\pi/L$, and the angular frequency ω can take the discrete values $\omega_j = jh_\omega$, where $h_\omega = 2\pi/T$. For the sake of simplicity, we use the following short notation for the summations:

$$Q(\boldsymbol{k},\ \omega) = \frac{h_x^2 h_t}{(2\pi)^3} \sum_{\boldsymbol{x},t} Q(\boldsymbol{x},\ t) e^{-i\boldsymbol{k}\cdot\boldsymbol{x}+i\omega t}. \tag{A2}$$

In this short notation, the inverse Fourier transform is

$$Q(\boldsymbol{x},\ t) = h_k^2 h_\omega \sum_{\boldsymbol{k},\omega} Q(\boldsymbol{k},\ \omega) e^{i\boldsymbol{k}\cdot\boldsymbol{x}-i\omega t}. \tag{A3}$$

Note that, in the continuous limit, these Fourier conventions are the same as in Gizon & Birch (2002).

APPENDIX B

DEFINITION OF TRAVEL TIME

In this appendix we give the motivation for the definition of travel time expressed by equation (3). For the sake of simplicity, we can assume that $C(\boldsymbol{x}_1, \boldsymbol{x}_2, t)$ is a continuous function of time: it can be Fourier interpolated onto an arbitrarily fine time grid (C is band-limited in frequency space). At fixed ϵ in the range (0, 1], the badness of fit between $C^\epsilon = \epsilon C + (1-\epsilon)C^{\rm ref}$ and the sliding reference cross-covariance $C^{\rm ref}$ is defined by

$$X_\pm^\epsilon(\boldsymbol{x}_1,\ \boldsymbol{x}_2,\ t) = \int_{-\infty}^{\infty} dt' f(\pm t') \left[C^\epsilon(\boldsymbol{x}_1,\ \boldsymbol{x}_2,\ t') - C^{\rm ref}(\boldsymbol{\Delta},\ t' \mp \epsilon t)\right]^2. \tag{B1}$$

The one-way travel times τ_+^ϵ and τ_-^ϵ are defined to be the time lags that minimize X_+ and X_-,

$$\tau_\pm^\epsilon(\boldsymbol{x}_1,\ \boldsymbol{x}_2) = \mathrm{argmin}_t\, X_\pm^\epsilon(\boldsymbol{x}_1,\ \boldsymbol{x}_2,\ t). \tag{B2}$$

This method for measuring travel times is a generalization of the case $\epsilon = 1$ employed by Gizon & Birch (2002) to measure travel times when $T \to \infty$, i.e., when C can be replaced by $E[C]$. This approach is borrowed from the geophysics literature (Zhao & Jordan 1998; Zhao et al. 2000).

The isolation window f enables us to fit separately the travel time for waves going from $\boldsymbol{x}_1$ to $\boldsymbol{x}_2$ (plus sign subscript) and the waves going from $\boldsymbol{x}_2$ to $\boldsymbol{x}_1$ (minus sign subscript). The function $f(t)$, which is 0 for $t < 0$, selects an interval around the arrival time of the wave packet. In the case of f-mode wave packets, the cross-covariance has only one branch, and we take $f(t)$ equal to the Heaviside step function. For acoustic waves there are multiple branches corresponding to multiple bounces off the surface between $\boldsymbol{x}_1$ and $\boldsymbol{x}_2$, and $f(t) = 1$ in a time interval around the first-bounce arrival time of the wave packet and 0 elsewhere.

When C is noisy (T is short) the parameter ϵ must be small enough that the envelope of C^ϵ is well defined. It can be shown numerically that there exists a value of ϵ below which the travel times τ^ϵ do not depend on ϵ. Thus, the limit $\epsilon \to 0$ provides a robust definition of travel time, whatever the noise level. In this limit X_+ and X_- always have well-defined minima.

The reference cross-covariance $C^{\rm ref}$ can be constructed from a model cross-covariance C^0 computed for a plane-parallel, horizontally homogenous standard solar model (see, e.g., Gizon & Birch 2002; Birch et al. 2004). For the purpose of measuring travel times, any model with a reasonable power spectrum will do. It can be shown that if $\epsilon = 1$ (appropriate for noiseless data), then the travel times returned by equation (B2) are independent of the amplitude of $C^{\rm ref}$. This is, however, not true for small ϵ-values, in particular, when $\epsilon \to 0$. This difficulty is a consequence of the fact that we are not fitting for the amplitude of the cross-covariance. For now, all we want is a meaningful definition of travel time to study realization noise in a quiet-Sun region. We choose $C^{\rm ref}$ such that its amplitude matches an estimate of the amplitude of $E[C]$, so that the amplitudes of $C^{\rm ref}$ and $E[C^\epsilon]$ will be similar in equation (B1). In the quiet Sun, it is reasonable to assume that the expectation of C can be approximated by its spatial average, i.e., $E[C] \sim \langle C \rangle$. Thus, we write $C^{\rm ref}(t) = A_+ C^0(t)$ for $t > 0$ and $C^{\rm ref}(t) = A_- C^0(t)$ for $t < 0$, where the normalization constants $A_\pm$ are such that

$$\int_{-\infty}^{\infty} f(\pm t') \left[C^{\rm ref}(\boldsymbol{\Delta},\ t')\right]^2 dt' = \int_{-\infty}^{\infty} f(\pm t') \langle C(\boldsymbol{x}_1,\ \boldsymbol{x}_2,\ t') \rangle C^{\rm ref}(\boldsymbol{\Delta},\ t')\, dt'. \tag{B3}$$

This normalization guarantees that $\tau_\pm^\epsilon$ are independent of ϵ when $C = \langle C \rangle$ and thus that the $\epsilon \to 0$ and $\epsilon = 1$ travel times are identical in this particular case.

To avoid numerical problems, we take the $\epsilon \to 0$ limit analytically. First we rewrite explicitly condition (B2), according to which τ_+^ϵ and τ_-^ϵ minimize the functions X_+ and X_- by requiring that the time derivative of $X_\pm$ vanish at times $\tau_\pm$:

$$\int_{-\infty}^{\infty} dt f(\pm t) \left[\epsilon C(\boldsymbol{x}_1,\ \boldsymbol{x}_2,\ t) + (1-\epsilon) C^{\rm ref}(\boldsymbol{\Delta},\ t) - C^{\rm ref}\left(\boldsymbol{\Delta},\ t \mp \epsilon\tau_\pm^\epsilon\right)\right] \dot{C}^{\rm ref}\left(\boldsymbol{\Delta},\ t \mp \epsilon\tau_\pm^\epsilon\right) = 0, \tag{B4}$$

where the overdot denotes the time derivative. In the limit of small ϵ, we can linearize the above equation to first order in ϵ and extract the travel times:

$$\tau_\pm(\boldsymbol{x}_1,\ \boldsymbol{x}_2) = \lim_{\epsilon\to 0+} \tau_\pm^\epsilon(\boldsymbol{x}_1,\ \boldsymbol{x}_2) = \mp\ \frac{\int_{-\infty}^{\infty} dt f(\pm t)\dot{C}^{\rm ref}(\boldsymbol{\Delta},\ t)\left[C(\boldsymbol{x}_1,\ \boldsymbol{x}_2,\ t) - C^{\rm ref}(\boldsymbol{\Delta},\ t)\right]}{\int_{-\infty}^{\infty} dt' f(\pm t')\left[\dot{C}^{\rm ref}(\boldsymbol{\Delta},\ t')\right]^2}\ . \tag{B5}$$

Hence, we obtain a linear relationship between $\tau_\pm$ and $C - C^{\rm ref}$ for $\epsilon \to 0$. For discrete times, the definition of travel times is expressed by equations (3) and (4) given in the text.

The center-to-annulus travel times $\tau(\boldsymbol{x}; \Delta)$ are measured in a similar way from $C_{\rm ann}(\boldsymbol{x}, \Delta, t)$. The only difference is that we use a reference cross-covariance $C^{\rm ref}_{\rm ann}(\Delta,\ t)$ such that its amplitude matches an estimate of the amplitude of $\langle C_{\rm ann}(\boldsymbol{x}, \Delta, t)\rangle$.

APPENDIX C

DETAILS OF THE TRAVEL-TIME COVARIANCE MODEL

Our starting point is the relationship between the cross-covariance C and the centered travel times $\tau_a - E[\tau_a]$:

$$\tau_a(\boldsymbol{x}_1,\ \boldsymbol{x}_2) - E[\tau_a(\boldsymbol{x}_1,\ \boldsymbol{x}_2)] = h_t \sum_t W_a(\boldsymbol{\Delta},\ t)\{C(\boldsymbol{x}_1,\ \boldsymbol{x}_2,\ t) - E[C(\boldsymbol{x}_1,\ \boldsymbol{x}_2,\ t)]\}. \tag{C1}$$

This is a generalization of equation (3) for arbitrary type, a, of travel times. Equation (C1) can be written in Fourier space as

$$\tau_a(\boldsymbol{x}_1,\ \boldsymbol{x}_2) - E[\tau_a(\boldsymbol{x}_1,\ \boldsymbol{x}_2)] = 2\pi h_\omega \sum_\omega W_a^*(\boldsymbol{\Delta},\ \omega)\{C(\boldsymbol{x}_1,\ \boldsymbol{x}_2,\ \omega) - E[C(\boldsymbol{x}_1,\ \boldsymbol{x}_2,\ \omega)]\}. \tag{C2}$$

The travel-time covariance function can thus be expressed as

$$\mathrm{Cov}\left[\tau_a(\boldsymbol{x}_1,\ \boldsymbol{x}_2),\ \tau_b(\boldsymbol{x}_1',\ \boldsymbol{x}_2')\right] = (2\pi h_\omega)^2 \sum_{\omega,\omega'} W_a^*(\boldsymbol{\Delta},\ \omega) W_b(\boldsymbol{\Delta}',\ \omega')\mathrm{Cov}\left[C(\boldsymbol{x}_1,\ \boldsymbol{x}_2,\ \omega),\ C(\boldsymbol{x}_1',\ \boldsymbol{x}_2',\ \omega')\right], \tag{C3}$$

in terms of the covariance of C and the weight functions W that are used to measure the travel times. Next we write the temporal Fourier transform of the cross-covariance function in terms of the Fourier transform of the observable:

$$C(\boldsymbol{x}_1,\ \boldsymbol{x}_2,\ \omega) = h_\omega \phi^*(\boldsymbol{x}_1,\ \omega)\phi(\boldsymbol{x}_2,\ \omega). \tag{C4}$$

To obtain this result, we ignored the correlations in the spectral domain introduced by the temporal window function, Win(t):

$$\frac{h_t}{T - |t|} \sum_{t'} \mathrm{Win}(t')\mathrm{Win}(t' + t) e^{i(\omega' - \omega'')t'} \approx \delta_{\omega',\omega''}, \tag{C5}$$

in accordance with the assumptions of the noise model (§ 4.1). Using equation (C4), we can express the covariance of C in terms of the covariance of products of the form $\phi^*\phi$,

$$\begin{aligned}\mathrm{Cov}\left[C(\boldsymbol{x}_1,\ \boldsymbol{x}_2,\ \omega),\ C(\boldsymbol{x}_1',\ \boldsymbol{x}_2',\ \omega')\right] = h_\omega^2 h_k^8 \sum_{\boldsymbol{k}_1,\boldsymbol{k}_2,\boldsymbol{k}_1',\boldsymbol{k}_2'} &\mathrm{Cov}\left[\phi^*(\boldsymbol{k}_1,\ \omega)\phi(\boldsymbol{k}_2,\ \omega),\ \phi^*(\boldsymbol{k}_1',\ \omega')\phi(\boldsymbol{k}_2',\ \omega')\right] \\ &\times \exp\left(-i\boldsymbol{k}_1\cdot\boldsymbol{x}_1 + i\boldsymbol{k}_2\cdot\boldsymbol{x}_2 + i\boldsymbol{k}_1'\cdot\boldsymbol{x}_1' - i\boldsymbol{k}_2'\cdot\boldsymbol{x}_2'\right).\end{aligned} \tag{C6}$$

The covariance of $\phi^*\phi$ involves the computation of fourth moments of ϕ. Using the assumption that the $\phi(\boldsymbol{k}, \omega)$ are independent complex random variables that are normally distributed, one can show

$$\begin{aligned}\mathrm{Cov}\left[\phi^*(\boldsymbol{k}_1,\ \omega)\phi(\boldsymbol{k}_2,\ \omega),\ \phi^*(\boldsymbol{k}_1',\ \omega')\phi(\boldsymbol{k}_2',\ \omega')\right] = {}& \delta_{\omega,\omega'}\left[\delta_{\boldsymbol{k}_1,\boldsymbol{k}_1'}\delta_{\boldsymbol{k}_2,\boldsymbol{k}_2'}\mathcal{P}(\boldsymbol{k}_1,\ \omega)\mathcal{P}(\boldsymbol{k}_2,\ \omega) - \delta_{\boldsymbol{k}_1,\boldsymbol{k}_2}\delta_{\boldsymbol{k}_2,\boldsymbol{k}_1'}\delta_{\boldsymbol{k}_1',\boldsymbol{k}_2'}\mathcal{P}(\boldsymbol{k}_1,\ \omega)^2\right] \\ &+ \delta_{\omega,-\omega'}\left[\delta_{\boldsymbol{k}_1,-\boldsymbol{k}_2'}\delta_{\boldsymbol{k}_2,-\boldsymbol{k}_1'}\mathcal{P}(\boldsymbol{k}_1,\ \omega)\mathcal{P}(\boldsymbol{k}_2,\ \omega) - \delta_{\boldsymbol{k}_1,\boldsymbol{k}_2}\delta_{\boldsymbol{k}_2,-\boldsymbol{k}_1'}\delta_{\boldsymbol{k}_1',\boldsymbol{k}_2'}\mathcal{P}(\boldsymbol{k}_1,\ \omega)^2\right],\end{aligned} \tag{C7}$$

where $\mathcal{P}(\boldsymbol{k},\ \omega) = E[|\phi(\boldsymbol{k},\ \omega)|^2]$ is the expected power spectrum and δ is the Kronecker delta function. We used the relation $\phi^*(\boldsymbol{k},\ \omega) = \phi(-\boldsymbol{k},\ -\omega)$ and the fact that the distribution of $|\phi|^2$ is exponential, so that $E[|\phi|^4] = E[|\phi|^2]^2$. We insert equation (C7) into equation (C6) to obtain the covariance of C in the form

$$\begin{aligned}\mathrm{Cov}\left[C(\boldsymbol{x}_1,\ \boldsymbol{x}_2,\ \omega),\ C(\boldsymbol{x}_1',\ \boldsymbol{x}_2',\ \omega')\right] = {}& \delta_{\omega,\omega'}\left[\mathcal{C}(\boldsymbol{x}_1' - \boldsymbol{x}_1,\ \omega)\mathcal{C}(\boldsymbol{x}_2 - \boldsymbol{x}_2',\ \omega) - h_k^2\mathcal{F}(\boldsymbol{\Delta} - \boldsymbol{\Delta}',\ \omega)\right] \\ &+ \delta_{\omega,-\omega'}\left[\mathcal{C}(\boldsymbol{x}_2' - \boldsymbol{x}_1,\ \omega)\mathcal{C}(\boldsymbol{x}_2 - \boldsymbol{x}_1',\ \omega) - h_k^2\mathcal{F}(\boldsymbol{\Delta} + \boldsymbol{\Delta}',\ \omega)\right],\end{aligned} \tag{C8}$$

where the functions $\mathcal{C}$ and $\mathcal{P}$ are defined by

$$\mathcal{C}(\boldsymbol{x},\ \omega) = h_k^2 \sum_{\boldsymbol{k}} h_\omega h_k^2 \mathcal{P}(\boldsymbol{k},\ \omega) e^{i\boldsymbol{k}\cdot\boldsymbol{x}}, \tag{C9}$$

and

$$\mathcal{F}(\boldsymbol{x}) = h_k^2 \sum_{\boldsymbol{k}} \left[h_\omega h_k^2 \mathcal{P}(\boldsymbol{k},\ \omega)\right]^2 e^{i\boldsymbol{k}\cdot\boldsymbol{x}}. \tag{C10}$$

The function $\mathcal{C}(\boldsymbol{x}, \omega)$ is the temporal Fourier transform of the expected cross-covariance function. The terms that involve the function $\mathcal{F}$ are much smaller than the others and can be neglected, since they go to 0 as L increases. Note that $h_\omega h_k^2 \mathcal{P}(\boldsymbol{k},\ \omega)$ is the power spectrum per unit area per unit time. We can now insert equation (C8) into equation (C3) to obtain the covariance of the travel times. The final result is given by equation (28) of § 4.2.

APPENDIX D

APPROXIMATE RESULTS

D1. POINT-TO-POINT *f*-MODE TRAVEL-TIME NOISE

In this section we estimate the standard deviation $\sigma_{\rm diff}^{\rm noise}$ of *f*-mode travel times. In the regime $\Delta > \lambda$ (far field) the variance of $\tau_{\rm diff}$ is approximately (see eq. [28])

$$\left[\sigma_{\rm diff}^{\rm noise}(\Delta)\right]^2 \simeq \frac{(2\pi)^3}{T} \sum_{\omega} h_\omega |W_{\rm diff}(\Delta,\ \omega)|^2 \mathcal{C}^2(\Delta = 0,\ \omega). \tag{D1}$$

Note that $\mathcal{C}(\Delta = 0,\ \omega)$ is the power spectral density of ϕ at any particular spatial pixel (eq. [C4]). In the *f*-mode case, we take the isolation window $f(t)$ to be the Heaviside step function, and thus the weight function $W_{\rm diff}$ can be written (Gizon & Birch 2002) as

$$W_{\rm diff}^*(\Delta,\ \omega) = \frac{-2i\omega C^{\rm ref}(\Delta,\ \omega)}{2\pi h_\omega \sum_{\omega'} \omega'^2 |C^{\rm ref}(\Delta,\ \omega')|^2}\ . \tag{D2}$$

For $\mathcal{C} \simeq C^{\rm ref}$, we have

$$\sigma_{\rm diff}^{\rm noise}(\Delta) \simeq \frac{2\left[\sum_\omega \omega^2 \mathcal{C}^2(\Delta,\ \omega) \mathcal{C}^2(\Delta = 0,\ \omega)\right]^{1/2}}{\sum_\omega \omega^2 \mathcal{C}^2(\Delta,\ \omega)}\ . \tag{D3}$$

In the far-field approximation the *f*-mode cross-covariance $\mathcal{C}(\Delta, \omega)$ can be written as

$$\mathcal{C}(\Delta,\ \omega) \simeq \sqrt{\frac{2}{\pi \kappa_r \Delta}}\, \mathcal{C}(\Delta = 0,\ \omega) e^{-\kappa_i \Delta} \cos\left(\kappa_r \Delta - \frac{\pi}{4}\right), \tag{D4}$$

where the wavenumber at *f*-mode resonance is $\kappa_r + i\kappa_i$. Specifically, $\kappa_r = \omega^2/g$ and $\kappa_i = \omega\Gamma/g$, where $g = 274$ m s^{-2} is the gravitational acceleration at the surface of the Sun and Γ is the FWHM of the *f*-mode ridge at frequency ω. The sums in equation (D3) can be approximated by noticing that the cosine in equation (D4) oscillates many times within the frequency width ξ of the envelope of $\mathcal{C}^2(\Delta = 0,\ \omega)$. The result is

$$\sigma_{\rm diff}^{\rm noise}(\Delta) \sim 2\pi\beta\, \frac{e^{\kappa_i \Delta}}{\omega_0} \sqrt{\frac{\kappa_r \Delta}{\xi T}}\,, \tag{D5}$$

where κ_i and κ_r are evaluated at the frequency that has maximum power, ω_0. The coefficient β is of order unity. For the example of § 5.1, Figure 5, we used $\omega_0/2\pi = 3.2$ mHz, $\xi/2\pi = 1$ mHz, $\beta = 0.8$, and $\Gamma/2\pi = 133$ μHz.

D2. CENTER-TO-ANNULUS TRAVEL-TIME NOISE

The point-to-point covariance $\mathrm{Cov}_{a,b}^{\rm noise}$ from equation (28) can be averaged over all the pairs of points that contribute to the center-to-annulus travel times. This averaging procedure involves the function $\aleph$, which defines the geometry of the annulus, as

described in § 2, equation (7). Assuming that $\mathcal{P}(\boldsymbol{k}, \omega)$ does not depend on the direction of $\boldsymbol{k}$, we obtain the following approximation to the noise covariance:

$$\mathrm{Cov}^{\mathrm{noise}}_{\alpha,\beta}(\boldsymbol{d},\ \Delta,\ \Delta') \approx \frac{(2\pi)^3}{T} \sum_{\omega} h_\omega W^*_\alpha(\Delta,\ \omega)\Big[W_\beta(\Delta',\ \omega)\mathcal{C}(d,\ \omega)\mathrm{I}(d,\ \Delta,\ \Delta',\ \omega) + W^*_\beta(\Delta',\ \omega)\mathrm{II}(d,\ \Delta',\ \omega)\mathrm{II}(d,\ \Delta,\ \omega)\Big]. \tag{D6}$$

The functions I and II are defined by

$$\mathrm{I}(d,\ \Delta,\ \Delta',\ \omega) = 2\pi h_\omega h_k^2 \int_0^\infty k\,dk\, e^{-w^2k^2}\mathcal{P}(k,\ \omega)J_0(kd)J_0(k\Delta)J_0(k\Delta'), \tag{D7}$$

$$\mathrm{II}(d,\ \Delta,\ \omega) = 2\pi h_\omega h_k^2 \int_0^\infty k\,dk\, e^{-k^2w^2/2}\mathcal{P}(k,\ \omega)J_0(k\Delta)J_0(kd). \tag{D8}$$

In deriving this result we used the approximation

$$\frac{\sum_{\boldsymbol{x}} \aleph(\|\,\boldsymbol{x}\,\| - \Delta)e^{i\boldsymbol{k}\cdot\boldsymbol{x}}}{\sum_{\boldsymbol{x}} \aleph(\|\,\boldsymbol{x}\,\| - \Delta)} \simeq e^{-w^2k^2/2}J_0(k\Delta), \tag{D9}$$

valid for $w \ll \Delta$ and $\aleph(\rho) = \exp(-\rho^2/2w^2)$. From equation (D6) for $\mathrm{Cov}_{\alpha,\beta}$ we can also obtain an approximation to the correlation $\mathrm{Cor}_{\alpha,\beta}$ and the standard deviation σ_α (see eqs. [26] and [25]).

In the particular case of *f*-modes, we can obtain a further approximation for the integrals that enter equation (D6), in the spirit of Appendix D.1. We find that the dispersion of the "oi" travel times (annulus averaging) and the "diff" travel times (point-to-point) are roughly related by

$$\sigma^{\mathrm{noise}}_{\mathrm{oi}}(\Delta) \sim \sigma^{\mathrm{noise}}_{\mathrm{diff}}(\Delta)\sqrt{\frac{e^{-\kappa_r^2w^2}(1 - e^{-2\kappa_i\Delta})}{\pi\kappa_r\Delta}}\,. \tag{D10}$$

The ratio $\sigma_{\mathrm{oi}}/\sigma_{\mathrm{diff}}$ goes down as the damping is reduced (through κ_i). When damping is large, averaging over the annulus simply reduces the noise level by a geometric factor of order $(\kappa_r\Delta)^{1/2} = (2\pi\Delta/\lambda)^{1/2}$, which is the square root of the number of wavelengths that fit in the circumference.

APPENDIX E

SPATIAL POWER SPECTRA OF POINT-TO-POINT TRAVEL TIMES

We compute the spatial Fourier transform of $\mathrm{Cov}_{a,a}(\boldsymbol{d})$ (see eq. [28]) with respect to the variable $\boldsymbol{d}$ at constant $\boldsymbol{\Delta} = \boldsymbol{\Delta}'$. We write the result as

$$S_a(\boldsymbol{k}) = \sum_{\omega} \mathcal{S}_a(\boldsymbol{k},\ \omega), \tag{E1}$$

where

$$\mathcal{S}_a(\boldsymbol{k},\ \omega) \propto \sum_{\boldsymbol{k}'} W_a(\boldsymbol{\Delta},\ \omega)^2\mathcal{P}(\boldsymbol{k}' + \boldsymbol{k}/2,\ \omega)\mathcal{P}(\boldsymbol{k}' - \boldsymbol{k}/2,\ \omega) + e^{2i\boldsymbol{k}'\cdot\boldsymbol{\Delta}}\big[W^*_a(\boldsymbol{\Delta},\ \omega)\big]^2\mathcal{P}(\boldsymbol{k}' + \boldsymbol{k}/2,\ \omega)\mathcal{P}(\boldsymbol{k}' - \boldsymbol{k}/2,\ \omega). \tag{E2}$$

From the above equation we can see that, at each frequency ω, $\mathcal{S}_a(\boldsymbol{k}, \omega)$ is like a low-pass filter with a cutoff wavenumber $k_c \approx 2k_\omega$, where k_ω is the maximum wavenumber at which there is significant power at frequency ω (for example, $k_\omega \approx \kappa_r$ for the *f*-mode case). The sum over frequencies, equation (E1), is dominated by terms with ω near the dominant frequency ω_0, because $\mathcal{S}_a$ scales with ω as $\mathcal{P}^4$, which is well localized around ω_0. This cutoff in the spectrum is seen clearly in Figures 7*c*, 9*c*, 12*c*, and 12*d*, as well as in the work of Jensen et al. (2003). In the spatial domain, the correlation length is $2\pi/k_c \approx \lambda/2$, where λ is the dominant wavelength in the filtered power spectrum.

REFERENCES

Baudin, F., & Korzennik, S. G. 1998, in Structure and Dynamics of the Interior of Sun and Sun-like Stars, Vol. 2, ed. S. Korzennik & A. Wilson (ESA SP-418; Noordwijk: ESA), 611

Birch, A. C., Kosovichev, A. G., & Duvall, T. L., Jr. 2004, ApJ, 608, 580

Duvall, T. L., Jr., D'Silva, S., Jefferies, S. M., Harvey, J. W., & Schou, J. 1996, Nature, 379, 235

Duvall, T. L., Jr., & Gizon, L. 2000, Sol. Phys., 192, 177

Duvall, T. L., Jr., & Harvey, J. W. 1986, in Seismology of the Sun and the Distant Stars, ed. D. O. Gough (Dordrecht: Reidel), 105

Duvall, T. L., Jr., Jefferies, S. M., Harvey, J. W., & Pomerantz, M. A. 1993, Nature, 362, 430

Duvall, T. L., Jr., et al. 1997, Sol. Phys., 170, 63

Gizon, L., & Birch, A. C. 2002, ApJ, 571, 966
Gizon, L., Duvall, T. L., Jr., & Larsen, R. M. 2000, J. Astrophys. Astron., 21, 339
Gough, D. O. 1996, in The Structure of the Sun, ed. T. Roca Cortés & F. Sánchez (Cambridge: Cambridge Univ. Press), 141
Gough, D. O., & Sekii, T. 2002, MNRAS, 335, 170
Hathaway, D. H., Beck, J. G., Bogart, R. S., Bachmann, K. T., Khatri, G., Petitto, J. M., Han, S., & Raymond, J. 2000, Sol. Phys., 193, 299
Jensen, J. M., Duvall, T. L., Jr., & Jacobsen, B. 2003, in Local and Global Helioseismology: The Present and Future, ed. S.-L. Huguette (ESA SP-517; Noordwijk: ESA), 315
Jensen, J. M., Duvall, T. L., Jr., Jacobsen, B., & Christensen-Dalsgaard, J. 2001, ApJ, 553, L193
Kosovichev, A. G. 1996, ApJ, 461, L55
Kosovichev, A. G., & Duvall, T. L., Jr. 1997, in SCORe'96: Solar Convection and Oscillations and their Relationship, ed. F. P. Pijpers, J. Christensen-Dalsgaard, & C. S. Rosenthal (Dordrecht: Kluwer), 241
Libbrecht, K. G. 1992, ApJ, 387, 712
Scherrer, P. H., et al. 1995, Sol. Phys., 162, 129
Schou, J. 1992, Ph.D. thesis, Aarhus Univ.
Toutain, T., & Appourchaux, T. 1994, A&A, 289, 649
Woodard, M. F. 1984, Ph.D. thesis, Univ. California, San Diego
———. 2002, ApJ, 565, 634
Woodard, M. F., & Fan, Y. 2004, ApJ, submitted
Zhao, L., & Jordan, T. H. 1998, Geophys. J. Int., 133, 683
Zhao, L., Jordan, T. H., & Chapman, C. H. 2000, Geophys. J. Int., 141, 558
Zhao, J., Kosovichev, A. G., & Duvall, T. L., Jr. 2001, ApJ, 557, 384

Note added in proof.—The noise covariance model given in § 4.2 (eqs. [28] and [29]) is only valid when the two travel times are obtained from the same signal ϕ (common Fourier filter F; see eq. [22]). Let us denote by $\tilde{\tau}$ the point-to-point travel time measured with a weight function $\tilde{W}$ from a signal $\tilde{\phi}$ filtered by $\tilde{F}$. It is easy to show that the covariance $\mathrm{Cov}[\tau_a, \tilde{\tau}_b]$ is obtained by replacing W_b by $\tilde{W}_b$ in equation (28) and $\mathcal{P}$ by $(\mathcal{P}\tilde{\mathcal{P}})^{1/2}$ in equation (29), where $\tilde{\mathcal{P}} = E[|\tilde{\phi}|^2]$. This generalization is useful when considering the covariance between p-mode travel times obtained with different phase-speed filters.